

Highlights

- Updated versions of GEISA 2015 and HITRAN 2016 line lists are validated using terrestrial solar occultation spectra from ACE-FTS.
- Spectroscopic parameters for CO₂ and H₂O are improved in both line lists.
- The primary difference we observe between the two line lists comes from O₃ absorption features near 3850 cm⁻¹ and from several CH₄ absorption lines in the regions 2800-3200 cm⁻¹ and 4000-4300 cm⁻¹.

Validation of the HITRAN 2016 and GEISA 2015 line lists using ACE-FTS solar occultation observations

K. S. Olsen^{a,*}, C. D. Boone^b, G. C. Toon^c, F. Montmessin^a,
A. A. Fedorova^d, O. Korablev^d, A. Trokhimovskiy^d

^a*Laboratoire Atmosphères, Milieux, Observations Spatiales (LATMOS), Université
Versailles St Quentin en Yvelines, Guyancourt 78280, France.*

^b*Department of Chemistry, University of Waterloo, Waterloo ON N2L 3G1, Canada.*

^c*Jet Propulsion Laboratory (JPL), California Institute of Technology, Pasadena CA
91109, USA.*

^d*Space Research Institute (IKI), Russian Academy of Sciences, Moscow 117997, Russia.*

Abstract

The ExoMars Trace Gas Orbiter (TGO) began its nominal science phase at Mars in April 2018, following releases of editions to two major spectroscopic line lists: GEISA 2015 (Gestion et Etude des Informations Spectroscopiques Atmosphériques: Management and Study of Atmospheric Spectroscopic Information), and HITRAN 2016 (High Resolution Transmission). This work evaluates both line lists over the spectral region between 2325–4350 cm⁻¹ using terrestrial solar occultation observations made by the Atmospheric Chemistry Experiment Fourier Transform Spectrometer (ACE-FTS). This spectral region is targeted on Mars by two complementary solar occultation instruments on TGO that will monitor temperature and pressure, aerosols,

*Corresponding author

Email addresses: kevin.olsen@latmos.ipsl.fr (K. S. Olsen), cboone@scisat.ca (C. D. Boone), geoffrey.c.toon@jpl.nasa.gov (G. C. Toon), franck.montmessin@latmos.ipsl.fr (F. Montmessin), fedorova@iki.rssi.ru (A. A. Fedorova), korab@iki.rssi.ru (O. Korablev), trokh@iki.rssi.ru (A. Trokhimovskiy)

Preprint submitted to Journal of Quantitative Spectroscopy and Radiative Transfer July 30, 2019

the abundance of CO₂, CO, H₂O, HDO, CH₄, and other undetected trace gases. Major updates to GEISA 2015 and HITRAN 2016, with respect to previous editions, have been focused on CO₂ absorption features in support of Earth-observing missions to monitor greenhouse. Since CO₂ is the dominant absorber on Mars, making up 96.5% of the atmosphere, validating the updated line lists is critically important before their deployment for ExoMars. We report that updated CO₂ parameters make significant improvements to spectral fits made when using both line lists. Several updates to H₂O lines in both line lists also show improvement. The primary difference we observe between the two line lists comes from O₃ absorption features near 3850 cm⁻¹ and from several CH₄ absorption lines in the regions 2800–3200 cm⁻¹ and 4000–4300 cm⁻¹. Because of these differences, we find that using HITRAN 2016 tends to result in better spectral fits, especially below 30 km, than using GEISA 2015 in this spectral region. Differences are strongly reduced with increasing altitude (> 40 km) as pressure and gas abundance falls off. It was also discovered that several new errors in both new editions of GEISA and HITRAN were introduced since the HITRAN 2012.

Keywords: ACE-FTS, HITRAN, GEISA, ExoMars, line-list

1. Introduction

New editions of two major spectroscopic line lists have been recently released: Gestion et Etude des Informations Spectroscopiques Atmosphériques: Management and Study of Atmospheric Spectroscopic Information (GEISA) in 2015 (Jacquinet-Husson et al., 2016); and High Resolution Transmission (HITRAN) in 2016 (Gordon et al., 2017). Here, we present a comparison

7 of spectral fits to solar occultation measurements of the Earth’s atmosphere
 8 made by the Canadian Space Agency’s (CSA’s) Atmospheric Chemistry Ex-
 9 periment (ACE) Fourier transform spectrometer (FTS) using both line lists.
 10 This work was motivated by the arrival of the European Space Agency (ESA)
 11 and Roscosmos’ ExoMars Trace Gas Orbiter (TGO) at Mars in October 2016.
 12 The TGO carries two infrared remote sensing instrument suites, the Atmo-
 13 spheric Chemistry Suite (ACS) (Korablev et al., 2018) and the Nadir and
 14 Occultation for Mars Discovery (NOMAD) (Vandaele et al., 2018). Both
 15 instrument suites carry channels dedicated to making solar occultation ob-
 16 servations at Mars in the infrared wavenumber range of 2325–4350 cm⁻¹.

17 The controversial observation of methane (CH₄) in the Martian atmo-
 18 sphere (Formisano et al., 2004; Krasnopolsky et al., 2004; Mumma et al.,
 19 2009; Webster et al., 2015, 2018; Giuranna et al., 2019) is one of the key mo-
 20 tivations of the ExoMars mission (Zurek et al., 2011; Vandaele et al., 2015;
 21 Korablev et al., 2018). NOMAD and ACS will search for CH₄ by making
 22 solar occultation observations of its ν_2 vibration-rotation band centred near
 23 3000 cm⁻¹, which hosts the strongest absorption features available to both
 24 instruments. A key benefit of searching for CH₄ in this region is that it is
 25 relatively clear of interfering absorption lines from CO₂. There is a recently-
 26 observed, weak vibration-rotation band of carbon dioxide (CO₂) that overlaps
 27 CH₄ in this region (Bertaux et al., 2008; Villanueva et al., 2008) and one of
 28 our specific objectives was to evaluate its spectroscopic parameters in GEISA
 29 2015 and HITRAN 2016.

30 ACS and NOMAD will also make detailed measurements of water vapour
 31 (H₂O), having the capability of distinguishing isotopologues. The ratio of

HDO to H₂O has been used as a critical indicator of the Martian climate in the ancient past (e.g., Encrenaz et al., 2018; Krasnopolsky, 2015). The relative abundance of HDO on Mars is enriched relative to Earth, which supports mechanisms for hydrogen escape from the atmosphere, which are preferential towards the lighter isotope (Clarke et al., 2017). ACS and NOMAD will be able measure the vertical structure of H₂O isotopologues, and monitor their ratios seasonally, spatially, and vertically.

In support of the study of Earth’s contemporary climate, and the carbon cycle, with the Orbiting Carbon Observatory (OCO-2) (Crisp et al., 2004, 2017), the Greenhouse gases Observing SATellite (GOSAT) (Yokota et al., 2009), and the Total Carbon Column Observing Network (TCCON) (Wunch et al., 2011), a large effort has been undertaken to refine and reduce the uncertainty of the spectroscopic parameters of CO₂. While the surface pressure of Mars is only between 550–720 Pa, roughly 0.5–0.7% of Earth’s, the volume mixing ratio of CO₂ is 0.965, or 2400 times that on Earth (400 ppmv). Therefore, CO₂ absorption lines in Mars solar occultation spectra will be deeper and broader than for spectra recorded at Earth, and small changes in the spectroscopic parameters may have a large impact on trace gas retrievals made at Mars.

Our goal was to evaluate the new CO₂, H₂O, and CH₄ parameters by looking at whether their impact when fitting terrestrial spectra was positive or negative. We have performed spectral fitting for 125 sets of ACE-FTS occultation spectra (resolution of 0.02 cm⁻¹) over 50 spectral windows covering the spectral range of 2430–4450 cm⁻¹ using the HITRAN 2012, HITRAN 2016, and GEISA 2015 line lists.

HITRAN 2016 and GEISA 2015 are compilations of data sources, many of which are shared. One of our most important results is that the updated CO₂ parameters for some of the stronger vibration-rotation bands, especially those centred at 3550 cm⁻¹ result in strongly improved spectral fits when using either HITRAN 2016 or GEISA 2015. However, we have also found that there are large differences in the spectroscopic parameters of ozone (O₃), CH₄, and H₂O between the two data sets, and that using HITRAN 2016 leads to improved spectral fits compared to GEISA 2015. This result is significant since methane is one of the strongest absorbers in the Earth’s atmosphere, and is one of the most variable gases. Methane is of key importance for TGO, as ACS and NOMAD both aspire to make its irregular and controversial detection in the Martian atmosphere definitive. However, at this time no methane features have been observed at Mars by TGO instruments (Korablev et al., 2019).

While individual contributions to the line lists are validated, they are often done in laboratory settings, observing controlled gas samples, rather than with observations of an atmosphere (e.g., Jacquinet-Husson et al., 2016; Gordon et al., 2017, and references therein). Bailey (2009) previously made a direct comparison between H₂O transitions in older versions of GEISA and HITRAN, and qualitatively showed their differences using modelled spectra for Venus at high temperatures and above 4000 cm⁻¹. A comprehensive validation of the GEISA line list was done using TCCON and the Infrared Atmospheric Sounding Interferometer (IASI) (Clerbaux et al., 2009) by Armante et al. (2016). They describe a technique used to determine whether spectroscopic parameters should be used to update the GEISA database based

82 on comparisons of computed spectra to observations. They specifically show
83 H₂O and HDO in the ExoMars region of interest and highlight improvements
84 since GEISA 2011. They also compare CH₄ lines above 6000 cm⁻¹ to HI-
85 TRAN 2012 and note an improvement to the residuals. This method was
86 used in the compilation of GEISA 2015 (Jacquinet-Husson et al., 2016).

87 A comprehensive validation of the HITRAN 2012 line list was undertaken
88 by Toon et al. (2016) using the MkIV balloon-borne FTS (Toon, 1991). They
89 divided the spectral region between 670–5620 cm⁻¹ into fitting windows and
90 quantitatively evaluated the best-fit residuals across the spectral range and
91 with altitude for several versions of HITRAN released since 2000. They
92 noted specific errors in the data base, where improvements were made, and
93 where previous versions performed better. Their work was influential on the
94 compilation of the latest version of HITRAN evaluated here (Gordon et al.,
95 2017). Updates to Toon et al. (2016) are included in Toon (2019) and include
96 evaluation of HITRAN 2016 and the TCCON internal line list, validation
97 with laboratory spectra, and a specific analysis of CO₂ features. This work
98 follows Toon et al. (2016) by using a similar quantitative evaluation technique
99 and covering part of the same spectral region.

100 2. HITRAN 2016

101 The HITRAN (high-resolution transmission molecular absorption) database
102 was first compiled for the Air Force Geophysics Laboratory (AFGL) by Mc-
103 Clatchey et al. (1973) and major updated editions have been released on a
104 four year cycle since 1992 (Rothman et al., 1992). The 2016 version of the HI-
105 TRAN database (Gordon et al., 2017) describes changes made since the 2012

106 edition (Rothman et al., 2013). Among the most significant additions to the
 107 database have been the inclusion of spectroscopic parameters for collision-
 108 induced broadening from non-nitrogen based atmospheres and for non-Voigt
 109 line profiles (Wilzewski et al., 2016). The need for line broadening param-
 110 eters in atmospheres primarily composed of gases other than N_2 has been
 111 motivated by extra-terrestrial spectroscopic applications, *e.g.*, Mars, which
 112 is 96% CO_2 . HITRAN 2016 includes a sparse set of broadening parameters
 113 for atmospheres composed of H_2 , He, or CO_2 for a subset of gases that in-
 114 cludes CO, OCS, SO_2 , NH_3 , HF and HCl, which are all sought at Mars by
 115 the ExoMars TGO. For very high-resolution applications, HITRAN 2016 also
 116 includes parameters for the speed-dependent Voigt, Galatry, and Hartman-
 117 Tran line shapes. These are again only available for a subset of wavenumbers
 118 and only for H_2O , CO, H_2 , O_2 , N_2O , HF and HCl. Because of the complexity
 119 of the newly included parameters, newly-developed online tools are now used
 120 to create user-defined database versions. The 2016 version also expands the
 121 list of available molecules with the addition of C_2N_2 and $COCl_2$. While the
 122 number of additional lines, and the number of lines for which more accurate
 123 measurements have been made, is vast, we will primarily focus on key species
 124 relevant to Earth and Mars: CO_2 , H_2O and CH_4 .

125 For CO_2 , Gordon et al. (2017) identifies the imperative for high-accuracy
 126 spectroscopic parameters driven by GOSAT, OCO-2, TCCON, and others,
 127 and identifies validated improvements between the 2008 and 2012 versions of
 128 the HITRAN database (Toon et al., 2016). The 2012 version of the database
 129 was largely built on theoretical fits of the effective Hamiltonian or effective
 130 dipole moments, compiled as the CDSD-296 database (Tashkun et al., 2015),

131 supplemented by higher-accuracy experimental measurements made by Toth
132 et al. (2007, 2008a,b). The line intensity calculations in CDS-296 have
133 high uncertainties ($\sim 20\%$) and two new sets of theoretical computation have
134 been produced: the Ames list (Huang et al., 2014) and the UCL-IAO list
135 (Zak et al., 2016). These have been extensively validated experimentally,
136 and Gordon et al. (2017) refers to 14 such studies that show that the UCL-
137 IAO list tends to be more accurate, and that the uncertainties for the 2016
138 version of HITRAN can be pushed down to the order of 0.5%. However, the
139 majority of the experimental work focuses on important CO_2 bands for Earth
140 observation (*e.g.*, for OCO-2) that lie outside the range of high-resolution
141 solar occultation experiments on TGO, above 5000 cm^{-1} (near 1.6 and $2\text{ }\mu\text{m}$).
142 Only laboratory measurements presented in Lyulin et al. (2012) and Durry
143 et al. (2010) cover the $2300\text{--}4400\text{ cm}^{-1}$ range, and the latter only does so near
144 3730 cm^{-1} . The 2016 HITRAN line list for CO_2 between $2300\text{--}4400\text{ cm}^{-1}$ is
145 a combination of CDS-296 theoretical calculations (Tashkun et al., 2015),
146 UCL-IAO or Ames theoretical calculations where better or newly available
147 (Huang et al., 2014; Zak et al., 2016), and laboratory measurements where
148 available and with low enough uncertainty (*e.g.*, Toth et al., 2008b; Durry
149 et al., 2010; Lyulin et al., 2012).

150 For H_2O , the HITRAN 2012 line list was made up of *ab initio* calculations
151 that comprised the BT2 line list (Barber et al., 2006), with updates, where
152 available, from calculations using a more accurate method (Lodi et al., 2011;
153 Lodi and Tennyson, 2012). Newer calculations using the methodology of Lodi
154 and Tennyson (2012) have been made as part of an effort by the International
155 Union of Pure and Applied Chemistry (IUPAC) task group (Tennyson et al.,

2009, and references therein). The new calculations have been validated experimentally by Birk et al. (2017) and the results have been used to update both the IUPAC database and the HITRAN line list. Extensive laboratory measurements have also been made for the German Aerospace Agency (DLR) in the spectral range between 1850–4000 cm^{-1} by Loos et al. (2017a,b). When available, these replace the calculated line strengths of IUPAC and Lodi and Tennyson (2012).

The CH_4 data in HITRAN 2012 was comprised of the data set described in Brown et al. (2013), which was a combination of theoretical calculations and experimental measurements. This data set replaced over 70% of the HITRAN 2008 line list for CH_4 (Rothman et al., 2009). However, analysis of high-resolution solar occultation measurements in the Earth’s atmosphere made by the MkIV interferometer (Toon, 1991) determined that there were still several errors and omissions in the HITRAN 2012 CH_4 data (Toon et al., 2016), especially in the spectral region of the ν_2 transition critical to Exo-Mars, near 3000 cm^{-1} . Errors that were identified were replaced by either the HITRAN 2008 values, or computations made by Tyuterev et al. (2013). Several laboratory studies have been recently undertaken, but the results have not yet been incorporated into the HITRAN line list, but an update to the 2016 edition is expected in the interim (Gordon et al., 2017).

3. GEISA 2015

The GEISA line list was first compiled in the early 1970s at the Laboratoire de Météorologie Dynamique (LMD) to support their radiative transfer investigations (Chédin et al., 1982). Key motivations for the compilation

were to include new gases important for planetary atmospheric applications, and to co-develop software tools to easily use the database. One distinguishing feature is to treat certain isotopologues with distinct symmetries as independent species (such as HDO for H₂O and CH₃D for CH₄) (Jacquinet-Husson et al., 2016). Comparing the available gases in current versions of GEISA and HITRAN, GeH₄, C₃H₈, C₃H₄, and C₆H₆ are unique to GEISA, while HOBr, O, H₂, and CS are unique to HITRAN. There are also several minor isotopologues of trace gases unique to both. Updates to GEISA are made after evaluating the relevance of new data, the efficiency of including it, and after undergoing a validation process as described in Armante et al. (2016).

For CO₂, the GEISA 2011 database was replaced by the CDSD-296 database (Tashkun et al., 2015). CDSD-296 is also the primary source of CO₂ parameters in the 2016 edition of HITRAN. GEISA also contains three isotopologues not contained in CDSD-296 from laboratory measurements by Jacquemart et al. (2012); Lyulin et al. (2012) (and others at higher wavenumbers than 4400 cm⁻¹).

Extensive updates to H₂O were made empirically for GEISA 2015 by a consortium of eight laboratories, nearly tripling the number of available lines since the 2011 edition. In the spectral region of interest to ExoMars (~2300–4400 cm⁻¹), these measurements were made by the Laboratoire Inter-Universitaire des Systèmes Atmosphériques (LISA), the Institute of Atmospheric Optics (IAO), and University College, London (Jacquinet-Husson et al., 2016). Updates to H₂¹⁶O come from (Coudert et al., 2014), and updates for H₂¹⁷O and H₂¹⁸O come from Lodi et al. (2011); Lodi and Tennyson (2012)

205 and the IUPAC efforts, which is the same source as for HITRAN 2016. These
206 were supplemented or updated by measurements made by Coudert and Che-
207 lin (2016). GEISA 2015 also newly includes lines for two isotopologues of
208 D₂O not included in HITRAN.

209 Updates to CH₄ in this spectral range mainly come from the work of
210 Niederer et al. (2013); Nikitin et al. (2013) which use the same methodology
211 as Brown et al. (2013) (HITRAN 2012). The validation work of Armante
212 et al. (2016) showed some imprecision in the new parameters, resulting in
213 some CH₄ lines from GEISA 2011 being retained.

214 4. Methodology

215 In this study, we break the wavenumber range of the ExoMars solar occul-
216 tation spectrometers up into discrete fitting windows and analyze terrestrial
217 solar occultation spectra recorded by ACE-FTS using the Jet Propulsion
218 Laboratory Gas Fitting (GFIT or GGG) software suite. 125 occultations
219 were analyzed. During an occultation, a series of observations of the sun
220 are made while the limb of the atmosphere lies between the solar disk and
221 the instrument. For each window, residuals were computed for each altitude
222 level. The means of the residuals were taken at levels of equal pressure, and
223 the root-mean-square (RMS) and standard deviation (σ) were computed for
224 each fitting window. The means of the residuals were taken, rather than
225 computing the residuals of mean spectra, due to variations in line depths be-
226 tween occultations, especially for CH₄ lines. In general, the lower the results
227 RMS of the mean residuals is, the more accurate the spectroscopic parame-
228 ters used in the fitting are. This methodology is very similar to that used by

229 Toon et al. (2016) who analyzed MkIV spectra.

230 ACE-FTS is a compact, double-pass interferometer with a spectral res-
231 olution of 0.02 cm^{-1} and a spectral range of $750\text{--}4400\text{ cm}^{-1}$. It has been
232 operating continuously in low-Earth orbit since 2003. The 125 ACE-FTS
233 occultations analyzed were recorded between 2004 and 2012 and are unre-
234 stricted in longitude and season. Most observations are at high latitudes
235 due to the ACE orbit (650 km with an inclination of 74°). A sequence of
236 measurements is made with an observation every 1–6.5 km, and on aver-
237 age every 4 km. Two detectors provide an simultaneous spectral range of
238 $750\text{--}4400\text{ cm}^{-1}$ (Bernath et al., 2005).

239 Spectral fitting in this study was done with GGG, which is also being
240 used to analyze solar occultation observations made by ACS on ExoMars.
241 GGG is developed from early Occultation Display Spectra (ODS) used by
242 the ATMOS FTS that flew on the space shuttle (Norton and Rinsland, 1991;
243 Irion et al., 2002). It is a robust software suite adaptable for solar occultations
244 (Toon, 1991; Toon et al., 2016; Olsen et al., 2015), ground based observations
245 (Wunch et al., 2011), or laboratory measurements. For each altitude and
246 each fitting window, GGG computes a spectrum from a set of parameters
247 that include the calculated optical path, vertical profiles of pressure and
248 temperature, and *a priori* gas volume mixing ratio (VMR) vertical profiles.
249 GGG then performs non-linear least squares fitting to adjust VMR scaling
250 factors (as well as other optional parameters such as continuum level and
251 frequency shift) to obtain a best fit. Retrieved VMR vertical profiles can be
252 obtained by inverting the matrix of VMR scale factors for each target gas at
253 each altitude, with the matrix of slant paths (Sen et al., 1996; Wunch et al.,

254 2011).

255 *A priori* temperature, pressure, and specific humidity vertical profiles
 256 were derived from National Centers for Environmental Prediction (NCEP)
 257 reanalysis data (Kalnay et al., 1996) up to 40 km. The US standard atmo-
 258 sphere was used above 40 km.

For this work, we consider the fitting residuals for each window and focus on three pressure levels where we take the means of the residuals: 0.052, 0.0029, and 0.00023 atm, corresponding to 20, 40 and 60 km respectively. For each occultation, fitting was performed at all altitudes and in all spectral windows. The closest altitude level to the predetermined pressure levels was identified. The residuals were computed for each window and the RMS and standard deviation were computed from the residual as:

$$\begin{aligned} \text{RMS}^2 &= \sum x_i^2 / N, \\ \sigma^2 &= \sum (x_i - \bar{x})^2 / (N - 1), \end{aligned} \quad (1)$$

259 where N is the number of spectral points, x_i is the residual value at the
 260 i^{th} spectral point, and \bar{x} is the mean of the residual. In general, for this
 261 application $\bar{x} \sim 0$ and $\text{RMS}^2 \sim \sigma^2$. For strong deviations between the
 262 computed and observed spectra, σ^2 will reflect the magnitude of deviations
 263 from the mean of the residuals, while the RMS will reflect the deviation from
 264 zero, which is the expected outcome for a good fit. Therefore, the presented
 265 results will use the RMS values.

266 The fitting windows used are given in Tables 1 and 2, and panel a in
 267 Figure 1 shows their distribution over a sample of ACE-FTS solar occultation
 268 transmission spectrum. Panels b–e in Figure 1 illustrate the locations and

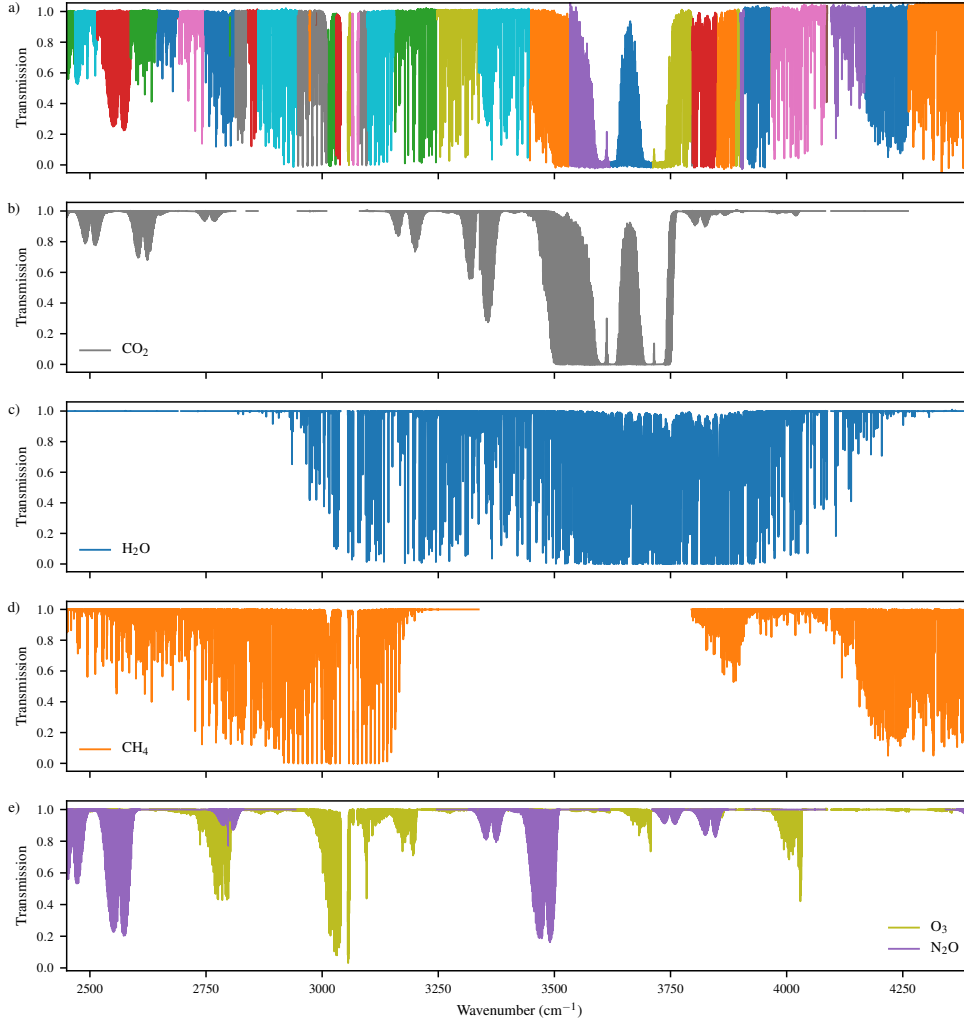


Figure 1: A look at ACE-FTS observations in the ExoMars spectral region of interest: a) mean ACE-FTS spectra at the 0.052 atm pressure level (near 20 km), the colours indicate different fitting windows; b) contributions from CO₂; c) contributions from H₂O; d) contributions from CH₄; e) contributions from O₃ and N₂O.

269 magnitudes of absorption features due to major gas species in the Earth's

270 atmosphere: CO₂, H₂O, CH₄, O₃, and N₂O.

271 5. Results

272 We begin with an overview of the differences between the HITRAN 2016
273 and GEISA 2015 line lists in the ExoMars spectral region of interest, 2325–
274 4350 cm⁻¹. Figure 2 shows mean ACE-FTS spectra averaged at three differ-
275 ent pressure levels corresponding to approximately 20, 40, and 60 km tan-
276 gent altitudes. Each primary panel, for each pressure level, shows the mean
277 ACE-FTS spectra, averaged over 125 occultations, for each fitting window
278 (Figure 2 does not show continuous ACE-FTS spectra). Shown over top of
279 the mean ACE-FTS spectra, is the mean of the calculated best fits for each
280 window when using the HITRAN 2016 line list (as an example). It is im-
281 portant to note that the noise level of the ACE-FTS spectra is not constant
282 with wavenumber (Boone et al., 2005), and the noise can be seen increasing
283 towards higher wavenumbers in Figure 2, even after averaging the ACE-FTS
284 spectra.

285 The secondary panels in Figure 2 show the mean residuals for each fitting
286 window at each pressure level. Shown are mean residuals when fitting with
287 HITRAN 2012, GEISA 2015, and HITRAN 2016. HITRAN 2012 tends to
288 have the largest numbers of errors and both newer line lists improve upon
289 it. The most significant errors are in the CO₂ band centred at 3508 cm⁻¹,
290 which were corrected in the 2016 edition (and not present in GEISA 2015).
291 Difficulty in fitting strong CO₂ lines in the region between 3500–3600 cm⁻¹
292 persists when using all three line lists, but this is also due to a strong increase
293 in detector noise in that region, visible in the mean spectra, especially at the

Table 1: List of spectral fitting windows used to evaluate the HITRAN 2016 and GEISA 2015 line lists with ACE-FTS solar occultation observations of the Earth’s atmosphere. Given for each fitting window are: centre wavenumber, window width, and gases fit in the window.

Centre $\tilde{\nu}$ (cm^{-1})	Width (cm^{-1})	Gases fit
2455.5	25.9	CO_2 , CH_4 , H_2O , N_2O , O_3
2491.5	47.9	CO_2 , CH_4 , H_2O , N_2O , O_3
2551.55	71.35	H_2O , CO_2 , O_3 , N_2O , CH_4
2615.74	56.2	CO_2 , CH_4 , H_2O , N_2O , O_3 , HCl , C_2H_6
2666.6	44.76	H_2O , CO_2 , O_3 , N_2O , CH_4 , HCl , C_2H_6
2689.8	0.62	HDO , CO_2 , O_3 , N_2O , CH_4
2692.76	0.55	HDO , CO_2 , O_3 , N_2O , CH_4
2708.17	0.54	HDO , CO_2 , O_3 , N_2O , CH_4
2722.25	52.0	CO_2 , CH_4 , C_2H_6 , H_2O , N_2O , O_3 , HCl , HDO
2780.74	65.15	CO_2 , CH_4 , C_2H_6 , H_2O , N_2O , O_3 , HCl , HDO
2801.6	0.49	HDO , CO_2 , O_3 , N_2O , CH_4
2825.0	22.95	H_2O , O_3 , N_2O , CH_4 , HDO , HCl
2849.15	24.55	HDO , CO_2 , H_2O , CH_4 , C_2H_6 , O_3 , N_2O , HCl
2904.43	85.10	H_2O , O_3 , N_2O , CH_4 , HDO , HCl , NO_2 , OCS
2973.65	1.21	C_2H_6 , CO_2 , H_2O , CH_4 , O_3
2978.2	62.0	CO_2 , CH_4 , C_2H_6 , C_2H_4 , H_2O , O_3 , HCl , HDO
2983.49	0.78	C_2H_6 , CO_2 , O_3 , CH_4
2986.74	0.58	C_2H_6 , CO_2 , O_3
2989.98	0.80	C_2H_6 , CO_2 , O_3 , CH_4
2993.52	1.23	C_2H_6 , CO_2 , O_3 , CH_4 , H_2O
3022.13	18.14	CH_4 , H_2O , C_2H_6 , C_2H_4 , O_3 , HCl
3035.08	9.2	CH_4 , H_2O , C_2H_6 , C_2H_4 , O_3
3057.72	5.1	CH_4 , H_2O , O_3
3065.86	3.35	CH_4 , H_2O , O_3
3077.36	2.54	CH_4 , H_2O , O_3

Table 2: List of spectral fitting windows used to evaluate the HITRAN 2016 and GEISA 2015 line lists with ACE-FTS solar occultation observations of the Earth’s atmosphere. Given for each fitting window are: centre wavenumber, window width, and gases fit in the window.

Centre $\tilde{\nu}$ (cm^{-1})	Width (cm^{-1})	Gases fit
3089.75	17.5	CH ₄ , H ₂ O, C ₂ H ₆ , C ₂ H ₄ , CO ₂ , O ₃
3126.65	58.0	CO ₂ , CH ₄ , C ₂ H ₄ , H ₂ O, O ₃ , HDO
3202.0	90.0	H ₂ O, CO ₂ , CH ₄ , O ₃ , HCN
3292.0	90.0	H ₂ O, CO ₂ , CH ₄ , O ₃ , HCN, N ₂ O
3391.15	108.6	CO ₂ , H ₂ O, C ₂ H ₂ , NH ₃ , HCN, N ₂ O, O ₃ , HDO
3489.0	86.0	H ₂ O, CO ₂ , O ₃ , N ₂ O
3577.0	86.0	H ₂ O, CO ₂ , O ₃ , N ₂ O, HNO ₃ , HDO
3665.0	86.0	H ₂ O, CO ₂ , O ₃ , N ₂ O, HNO ₃ , HDO
3753.0	86.0	H ₂ O, CO ₂ , O ₃ , N ₂ O, HF, HDO
3798.8	7.46	H ₂ O, CO ₂ , CH ₄ , O ₃
3822.5	51.0	CO ₂ , H ₂ O, N ₂ O, O ₃ , CH ₄ , HF, HDO
3869.14	42.0	H ₂ O, CO ₂ , O ₃ , N ₂ O, CH ₄ , HF, HDO
3895.36	10.18	H ₂ O, CO ₂ , CH ₄ , O ₃
3903.93	6.17	H ₂ O, CO ₂ , CH ₄ , O ₃
3936.15	58.0	CO ₂ , H ₂ O, N ₂ O, O ₃ , CH ₄ , HF, HDO
3967.79	2.0	H ₂ O, CO ₂ , CH ₄ , O ₃
4026.0	114.0	H ₂ O, CO ₂ , O ₃ , N ₂ O, CH ₄ , HF, CO
4085.69	3.4	HDO, CO, H ₂ O, O ₃ , CH ₄
4115.21	5.62	HDO, CO, O ₃ , CH ₄
4128.34	9.53	HDO, CO, H ₂ O, O ₃ , CH ₄
4132.1	72.5	CO, H ₂ O, CO ₂ , CH ₄ , O ₃
4214.2	94.1	CO, H ₂ O, CO ₂ , CH ₄ , O ₃
4300.4	76.6	CO, H ₂ O, CH ₄ , O ₃
4377.0	75.4	H ₂ O, O ₃ , CH ₄ , N ₂ O, CO
4436.2	42.6	CO ₂ , H ₂ O, CH ₄

294 lowest pressure level.

295 In general, HITRAN 2016 performs better than GEISA 2015, and larger
296 mean residuals are seen in Figure 2. The largest differences are observed the
297 lowest pressure levels, while both line lists perform similarly at higher tan-
298 gent altitudes. This suggests that the errors are related to either increased
299 pressure and pressure broadening at lower altitudes, or (and) that the mag-
300 nitude of the errors are related to line depth, and that when the line depths
301 are small, the errors are less than the instrument noise. When CH_4 or CO_2
302 lines are saturated, the residuals show the negative impact of untreated line
303 mixing, which was not implemented in this spectral region for this study, but
304 is available in GGG (Mendonca et al., 2016). Key areas that GEISA 2015
305 has difficulty with relative to HITRAN 2016 are between $2700\text{--}3200\text{ cm}^{-1}$,
306 when strong CH_4 lines absorb totally, between $4100\text{--}4300\text{ cm}^{-1}$, where errors
307 are related to O_3 lines and also CH_4 lines (shown in the following section).
308 These are also errors near 3800 cm^{-1} related to H_2O . Fitting the strong CO_2
309 lines between $3500\text{--}3700\text{ cm}^{-1}$ is challenging for GGG using any line list,
310 as shown in Figure 2, especially the middle pressure level. The ν_1 band of
311 HNO_3 is located in this region which is significant at 20 km.

312 At lower wavenumbers, where detector noise is lowest, there are system-
313 atic features observable in the mean residuals when using either line list.
314 Near 2550 cm^{-1} , this is related to line widths in an N_2O absorption band.
315 Near 2650 cm^{-1} , there is an observed absorption band of HNO_3 that is not
316 included in either line list. Several HNO_3 bands are observable in ACE-FTS
317 spectra that are not contained in the HITRAN or GEISA line lists. Weaker
318 bands result in an apparent baseline curvature, while stronger bands show

319 a distinct vibration-rotation band structure in the residuals. Examples are
320 shown in the following section.

321 Figure 3 shows the mean RMS for each fitting window, at each pressure
322 level. The RMS was computed for each ACE-FTS occultation in a given
323 window, and shown are the means of the RMS values, with the standard
324 deviation of the mean. At the highest pressure level (top panel, near 60 km),
325 all three line lists perform similarly. In the middle pressure level, near 40 km,
326 we observe strong increases in the mean RMS values, and their uncertainties,
327 where line depths extend beyond 50%, just above 3500 cm^{-1} due to CO_2 ,
328 and near 3000 cm^{-1} due to CH_4 . At the lowest pressure level, the RMS
329 uncertainties increase strongly for all windows, and the differences between
330 line lists become most apparent. At this level, we see deviations between
331 HITRAN 2012 and 2016, at the same locations observed in Figure 2. This
332 analysis also supports the observations made from Figure 2 regarding GEISA
333 2015. Specific examples and windows are explored in the following section.

334 6. Specific examples

335 6.1. $2440 - 2660\text{ cm}^{-1}$: N_2O and HNO_3

336 The spectral region between $2440 - 2660\text{ cm}^{-1}$ was covered by four broad
337 fitting windows centred at 2455.5 , 2491.5 , 2551.55 , and 2615.74 cm^{-1} . This
338 region is characterized primarily by the P and R branches of two vibration-
339 rotation bands of N_2O , centred near 2462 and 2562 cm^{-1} , and two vibration-
340 rotation bands of CO_2 , centred near 2501 and 2614 cm^{-1} . For these bands, all
341 three spectroscopic line lists perform similarly. In the 2491.5 cm^{-1} window,
342 small, but visible, improvements are apparent where CO_2 lines are present in

343 the two updated editions of the line lists when compared to HITRAN 2012.

344 Both the GEISA 2015 and HITRAN 2016 line lists perform almost equiv-
345 alently in this region. However, there are apparent problems in the fitting,
346 and these problems persist in both data sets. At the lower pressure level, the
347 N₂O fits produce large mean residuals whose shape is indicative of errors in
348 line width. These errors do not persist at the higher pressure levels and are
349 likely due to errors in the broadening parameters in the line lists. The mean
350 ACE-FTS spectra and mean residuals for the 2551.55 cm⁻¹ window, which
351 are shown in Figure 4. The lines in this window are mainly due to N₂O, with
352 some CH₄ lines throughout, and the edge of an *R* branch of CO₂ on the left
353 side.

354 Figure 5 shows the same information as Figure 4, but for the 2615.74 cm⁻¹
355 window. Again, both the GEISA 2015 and HITRAN 2016 line lists perform
356 equivalently, and, again, there are systematic differences between the obser-
357 vations and the computed spectra. These differences are due to HNO₃ lines
358 not included in either line list. The broad curvature of the baseline in the
359 residuals is due to a weaker band, while the distinct peaks to the right side
360 of Figure 4 are the *P* branch of a stronger HNO₃ vibration-rotation band.
361 There is a corresponding *R* branch in the adjacent 2666.6 cm⁻¹ window. The
362 feature of another weak HNO₃ band is also present in the 2491.5 cm⁻¹ win-
363 dow, and stronger missing lines are seen in the 2978.2 cm⁻¹ window, between
364 2985–3010 cm⁻¹, and in the 3391.15 cm⁻¹ window, between 3390–3415 cm⁻¹.
365 That these are due to HNO₃ is verified by measurements made for the line list
366 distributed by the Pacific Northwest National Laboratory (PNNL) (Sharpe
367 et al., 2004; Johnson et al., 2010). Supplementary HNO₃ line lists are used

368 for ACE-FTS and TCCON retrievals.

369 *6.2. 2660 – 3440 cm⁻¹: CH₄*

370 This wavenumber region is characterized by strong CH₄ absorption fea-
371 tures, but also contains important bands of O₃, N₂O and CO₂. This region
372 was covered by several narrow windows and 12 wide windows ranging in
373 width between 18–108 cm⁻¹. The first window centred at 2722.25 cm⁻¹ fea-
374 tures three strong CH₄ lines, and many associated weaker lines, and there are
375 significant residual errors about each due to unaccounted line mixing. Toon
376 et al. (2016) pointed out a positional error in a CH₄ line at 2742.3 cm⁻¹
377 that was introduced into HITRAN 2012 after the 2008 version. This error
378 is present in GEISA 2015 and HITRAN 2016, and is shown in Figure 6a.
379 While positive changes have been made to the HITRAN 2016 line list, cor-
380 recting the positional error, strong residual features remain, but these are
381 most likely due to unaccounted line mixing for such strong lines fit at a low
382 altitude. This window also features several weak O₃ lines that are well fit by
383 both line lists, except a small region around 2705–2710 cm⁻¹ where fitting
384 with GEISA 2015 results in larger mean residuals than fitting with HITRAN
385 2016, on the order of 0.005.

386 The window centred at 2780.74 cm⁻¹ contains weaker CH₄ lines and a
387 large O₃ band. Both line lists perform similarly here, but there is what
388 appears to be a single missing line in the GEISA 2015 list. This is an ozone
389 line at 2773.15 cm⁻¹ that is not missing, but has an error in line strength,
390 shown in Figure 6b. Toon et al. (2016) pointed out an error in position in an
391 O₃ resonance transition at 2761.42 cm⁻¹ that is seen in HITRAN 2012 and
392 GEISA 2015, but has been corrected in HITRAN 2016. However, there are

new O₃ positional errors at 2763.86 and 2798.0 cm⁻¹ in the HITRAN 2016 line list that were not present in HITRAN 2012.

The fitting window centred at 2825.0 cm⁻¹ presents one of the largest discrepancies between HITRAN 2016 and GEISA 2015. The mean ACE-FTS spectra and mean residuals when fitting with the three line lists are shown in Figure 7 for the lowest pressure level. These discrepancies are characteristic of the strong CH₄ lines throughout this region, and the systematic differentiation between fitting results using the two line lists is seen in Figure 3. There is little difference between the two versions of HITRAN, and both result in mean residual errors on the order of ± 0.01 about strong CH₄ lines. In several positions, however, when fitting with GEISA 2015, these residuals can be twice as large.

Windows centred at 2849.15, 2904.43, 2978.2 cm, and 3126.65 cm⁻¹ are similar to those preceding, predominantly featuring strong CH₄ lines, with line mixing errors apparent in the mean residuals when using either line list, but the largest residuals are found when using GEISA 2015. In the 2978.2 cm⁻¹ window, there are several saturated (at low altitude) CH₄ lines, and the beginning of a broad, strong band of O₃ lines, but also a set of HNO₃ lines that are missing in both line lists.

The 3022.13 cm⁻¹ window contains a mixture of strong O₃ and CH₄ lines. There is an opaque region about 5 cm⁻¹ wide at the lower pressure level, which is the *Q*-branch of this CH₄ band. This feature is critically important for ExoMars, as it is the strongest and broadest CH₄ feature in the available wavenumber range, and where the ExoMars instruments will focus their search for a CH₄ signature. Mean residuals on the right side of

418 the Q -branch (3018 cm^{-1}) are nearly equivalent when using GEISA 2015 or
 419 HITRAN 2016. On the left side (3015 cm^{-1}), mean residuals when using
 420 GEISA 2015 are larger than when using HITRAN 2016 by 0.01–0.02. Most
 421 of the fitting differences in this region can be attributed to CH_4 , but there is
 422 also a weaker HCl line at 3014.4 cm^{-1} that contributes to these differences.
 423 Note that the residuals for both line lists are significant (~ 0.002) even at
 424 the highest pressure level (near 60 km), where line depths are much weaker
 425 and only extend to 0.9. Of particular interest to ExoMars is the recently
 426 observed, weak CO_2 band centred near 3000 cm^{-1} that overlaps with these
 427 strong CH_4 features (Bertaux et al., 2008; Villanueva et al., 2008). This
 428 band is not visible in terrestrial solar occultation observations, its lines are
 429 too weak relative to the abundant absorption features of CH_4 and O_3 .

430 Figure 8 shows the mean spectra and mean residuals for fitting window
 431 3089.75 cm^{-1} . This region contains a set of three CH_4 lines near 3090 cm^{-1}
 432 that are poorly fit with either line list. When using HITRAN 2012 and
 433 HITRAN 2016, the magnitude of the mean residuals is 0.04, which is on the
 434 order of the line mixing errors seen when fitting stronger lines. When using
 435 GEISA 2015, the mean residuals are 50% larger. Figure 8 also shows a pair
 436 of saturated CH_4 lines, and fitting errors characteristic of such lines.

437 The window centred at 3126.65 cm^{-1} has some of the strongest CH_4 lines,
 438 and, therefore, the largest residuals. GEISA 2015 and HITRAN 2016 perform
 439 similarly here. The window centred at 3202.0 cm^{-1} contains the right edge of
 440 $\text{CH}_4\ \nu_2$ band. At higher wavenumbers, H_2O absorption becomes dominant.
 441 This window also features overlapping CO_2 and O_3 bands, the edge of the
 442 strong CH_4 band, and several water vapour lines. The 3292.0 cm^{-1} window

contains H₂O and CO₂ lines, with an H₂O line strength error at 3254.15 cm⁻¹ that has been reduced between HITRAN 2012 and HITRAN 2016, but is still significant in both HITRAN 2016 and GEISA 2015. This window contains several other H₂O lines where significant improvements were made to both line lists since HITRAN 2012 (e.g., at 3273.4 and 3276.5 cm⁻¹). The 3391.15 cm⁻¹ window is similar, but hosts another set of HNO₃ lines missing from both line lists. There is also an H₂O line strength error at 3367.65 cm⁻¹ in both GEISA 2015 and HITRAN 2016 that was not significant in HITRAN 2012.

6.3. 3440 – 3770 cm⁻¹: CO₂

This region was covered by five wide windows centred at 3391.15, 3489.0, 3577.0, 3665.0, and 3753.0 cm⁻¹. These windows cover the strongest CO₂ vibration-rotation bands observed by the ExoMars instruments. Throughout this region, there are only small differences between fits using GEISA 2015 and HITRAN 2016. However, there are significant improvements to several lines throughout since HITRAN 2012. Figure 9 shows the mean spectra and residuals for the window centred at 3489.0 cm⁻¹, where the most dramatic improvement is seen. The spectroscopic parameters for an entire band have been updated, resulting in significant improvements to fitting.

6.4. 3770 – 4080 cm⁻¹: H₂O

This spectral region, covered by four broad fitting windows centred at 3822.5, 3869.14, 3936.15, and 4026.0 cm⁻¹, features the strongest set of water vapour lines in the ExoMars region of interest. It is in this region where we again find that spectral fitting with the HITRAN 2016 results in smaller

467 residuals than when using GEISA 2015, as seen in Figure 3. Figure 10
 468 shows the window centred at 3869.14 cm^{-1} . The primary features are broad,
 469 saturated H_2O lines, but there are also many smaller CH_4 and N_2O lines,
 470 and many very weak lines from CO_2 and O_3 . The lines where fitting with
 471 GEISA 2015 resulted in systematic residual errors are largely attributable
 472 to weaker O_3 lines. Similar behaviour is seen in the window centred at
 473 3822.5 cm^{-1} , where several O_3 lines are not contained in GEISA 2015. Note
 474 the marked improvement in the strong H_2O line between HITRAN 2012 and
 475 the newer line lists near 3886 cm^{-1} , as shown in Figure 6c, but clearly visible
 476 in Figure 10.

477 The two windows at 3936.15 and 4026.0 cm^{-1} show improvements over
 478 the previous two windows when comparing GEISA 2015 and HITRAN 2016.
 479 The 3936.15 cm^{-1} window contains a portion of an O_3 *P*-branch. Significant
 480 residuals when using GEISA 2015 are from widely spaced CH_4 lines (e.g., at
 481 3912.15 , 3914.6 , and 3914.9 cm^{-1}), rather than O_3 . Two of these features
 482 near 3914.6 cm^{-1} are shown in Figure 6d. There is an H_2O line strength
 483 error in the HITRAN 2016 line list at 3925.15 cm^{-1} that was not present
 484 in HITRAN 2012, nor GEISA 2015. The 4026.0 cm^{-1} window hosts an O_3
 485 band, for which all line lists have difficulty accurately fitting over the region
 486 of the *Q*-branch. The O_3 band in this region is much better characterized by
 487 GEISA 2015 than that covered by the 3822.5 and 3869.14 cm^{-1} windows, but
 488 there remain small discrepancies in some minor CH_4 lines, especially towards
 489 the right edge of the window at 4080.65 and 4082.8 cm^{-1} .

490 6.5. 4080 – 4420 cm^{-1} : CH_4

491 Above 4100 cm^{-1} , the ACE-FTS noise increases, as can be seen in Fig-
492 ure 2, and it becomes difficult to evaluate the line lists further. This region
493 is characterized by a decreasing density of H_2O lines, increasingly stronger,
494 and more dense CH_4 absorption features, and a band of broadly spaced CO
495 lines. We evaluated five wide fitting windows in this region centred at 4132.1,
496 4214.2, 4300.4, 4377.0, and 4436.2 cm^{-1} . At 4115.65 cm^{-1} , a CH_4 line miss-
497 ing in HITRAN 2012, as identified by Toon et al. (2016), was added (also
498 included in GEISA 2015). There are CH_4 line strength errors in the GEISA
499 2015 line list at 4133.35 cm^{-1} and 4103.2 cm^{-1} that result in mean residuals
500 on the order of 0.1 at lower pressure levels. The latter is also apparent in
501 HITRAN 2016, despite not being present in HITRAN 2012.

502 As shown in Figure 3, the mean RMS values dramatically increase in this
503 spectral region for all evaluated line lists. At the lowest pressure level, fitting
504 with HITRAN 2016 results in the smallest residuals and the lowest mean
505 RMS values. It must be noted that the magnitude of the difference between
506 results using HITRAN 2016 and GEISA 2015 is on the order of the difference
507 between changing pressure levels, and that is only $\sim 1/5$ of the magnitude
508 of the mean RMS. Therefore, errors due to differences in the spectroscopic
509 parameters are much, much smaller than the noise level of the instrument in
510 this region.

511 The window centred at 4214.2 cm^{-1} features the most dramatic difference
512 between fitting using GEISA 2015 and fitting using HITRAN 2016. Mean
513 residuals with magnitudes greater than 0.1 come from several CH_4 lines near
514 4208, 4229, and 4255 cm^{-1} .

515 7. Conclusions

516 This study was motivated by the release of two new editions of spectro-
517 scopic line lists, the 2015 version of GEISA and the 2016 version of HITRAN,
518 and the launch and arrival of the ExoMars Trace Gas Orbiter as Mars,
519 equipped with two suits of spectroscopic instruments dedicated to charac-
520 terizing the Martian atmosphere. The largest efforts made recently towards
521 updating infrared spectroscopic databases has been in support of terrestrial
522 greenhouse gas observatories such as OCO-2, GOSAT, and TCCON. Since
523 the Martian atmosphere is composed of 96.5% CO₂, these updates are very
524 significant for the ExoMars mission. Our objective was to validate the two
525 line lists in the range of 2325–4350 cm⁻¹ by examining spectral fitting results
526 for terrestrial solar occultation observations made by ACE-FTS.

527 This work follows that of Toon et al. (2016) who compared different
528 versions of HITRAN, up to the 2012 release, in the spectral range of 670–
529 5620 cm⁻¹ using the solar occultation measurements made by the MkIV FTS.
530 They identified several errors in HITRAN 2012, some persisting from previ-
531 ous releases, and others newly introduced. The analysis in Toon et al. (2016)
532 is expanded in Toon (2019), which includes a detailed analysis of HITRAN
533 2016 using laboratory and solar occultation spectra. Because spectroscopic
534 parameters taken from previous HITRAN versions for some gases in some
535 spectral regions perform better, and because HITRAN may be incomplete
536 in some spectral regions (*e.g.*, HNO₃), the TCCON and GGG development
537 teams maintain a custom line list, as do other spectroscopic analysis teams,
538 such as ACE-FTS.

539 The 2016 edition of the HITRAN line list addressed several errors identi-

540 fied in the 2012 edition by Toon et al. (2016), such as the positional error in an
541 O₃ resonance transition at 2761.42 cm⁻¹ (still persists in GEISA 2015). We
542 have observed, however, a few minor errors introduced into HITRAN 2016
543 since the 2012 edition, such as the H₂O line strength errors at 3367.65 cm⁻¹
544 (also in GEISA 2015) and 3925.15 cm⁻¹.

545 For ExoMars, the gases of primary interest are CO₂, H₂O, CO, and CH₄.
546 Changes to line position and strength have been made to CO₂ lines across
547 our spectral region. For terrestrial spectra, the strongest improvements seen
548 in fitting coincide with the strongest absorption features, and the greatest
549 improvement is seen between 3470–3530 cm⁻¹ for both GEISA 2015 and
550 HITRAN 2016. In no region were increased residuals seen for CO₂ lines
551 when using the updated line list editions when compared to HITRAN 2012.
552 In the terrestrial observations, we also observe significant improvements to a
553 subset of H₂O lines, especially at higher wavenumbers, such as near 3093.7
554 or 3885.5 cm⁻¹. With the exception of individual CH₄ line errors, little
555 difference is observed in the CH₄ or CO transitions in this spectral region
556 between HITRAN 2012 and 2016.

557 Of key interest to us was the CO₂ vibration-rotation band centred at
558 2982 cm⁻¹ and partially overlapping the critically important CH₄ ν_2 band.
559 When comparing synthetic spectra generated with HITRAN 2016 or GEISA
560 2015, significant differences in these lines are seen. This band is absent from
561 GEISA 2015, but present in HITRAN 2012 and 2016. The lines included in
562 HITRAN 2016 have significantly increased line strengths relative to HITRAN
563 2012. Unfortunately, in terrestrial observations, these lines are too weak
564 relative to interfering species, especially CH₄, and noise. It is not observed

565 in the ACE-FTS spectra examined here above background noise levels, so
566 residuals between spectral fits using HITRAN 2012 and 2016 have not been
567 compared.

568 A critical difference between the application of spectroscopic calculations
569 for Earth and Mars is that because the Martian atmosphere is predom-
570 inantly CO₂ rather than N₂, the collision-induced broadening parameters
571 computed for HITRAN and GEISA will not be applicable to the Martian at-
572 mosphere. There is ongoing work to determine spectroscopic parameters for
573 a CO₂-rich atmosphere: *e.g.*, Gamache et al. (2016); Devi et al. (2017) for wa-
574 ter vapour; and Li et al. (2015) for CO. However, this study does not attempt
575 to validate these parameters, nor does it evaluate the CO₂ self-broadening
576 parameters.

577 When comparing the 2015 version of the GEISA line list to the latest,
578 2016, release of HITRAN, we observe that lower RMS values are found for
579 residuals from the majority of the spectral windows between 2325–4350 cm⁻¹
580 used here. We find that these are primarily due to differences in line strength
581 or position for strong O₃ and CH₄ lines. There are some minor errors in
582 specific lines noted as well.

583 We were surprised to find a large number of O₃ lines missing from GEISA
584 2015 in the 3830–3870 cm⁻¹ region that were present in HITRAN 2012.
585 The primary source of O₃ lines both HITRAN 2016 and GEISA 2015 is
586 the Spectroscopy and Molecular Properties of Ozone (S&MPO) informa-
587 tion system (Babikov et al., 2014) maintained by Reims University and the
588 Institute of Atmospheric Optics (Tomsk). For GEISA 2015, new measure-
589 ments of lines around this region were made at Reims University by Barbe

et al. (1997, 2012), but those lines precisely between 3830–3870 cm^{-1} are attributed to a private communication from Barbe (2011). O_3 line parameters in HITRAN 2016 are also included in the S&MPO database. In the region 3623–4229 cm^{-1} , HITRAN also includes an updated hot band from Barbe et al. (2013).

Our analysis fit the hydrogen halides HCl (between 2600–3050 cm^{-1}) and HF (between 3700–4100 cm^{-1}). Parameters for these gases were not updated in the 2011 or 2015 editions of GEISA, but new calculations were implemented in the 2012 edition of HITRAN (Li et al., 2013). The result is differences in line position when performing spectral fitting with HITRAN 2016 or GEISA 2015. Mean differences are very small relative to the noise of the ACE-FTS observations, less than 1%, with HITRAN 2016 performing slightly better at these line locations (*e.g.*, 2925.9 cm^{-1} or 2944.93 cm^{-1} for HCl, and 3877.7 cm^{-1} or 3920.3 cm^{-1} for HF).

In conclusion, we have noted consistent improvement in both line lists since HITRAN 2012, have noted errors and deficiencies in both line lists where found, and we hope that the collaborations in charge of both line lists will find this analysis useful when compiling the next release. However, for the purposes of the ExoMars TGO ACS and NOMAD instruments, we recommend HITRAN 2016 for use. HITRAN 2016 shows marked improvement over HITRAN 2012 in CO_2 and H_2O transitions (as does GEISA 2015). GEISA 2015 currently produces larger residuals for strong CH_4 lines that are critical for ExoMars, while an important CO_2 band centred at 2982 cm^{-1} has not yet been introduced.

614 8. Acknowledgements

615 All spectral fitting was performed by KSO using the GGG software suite.
616 The ACE-FTS spectra were provided by CDB, who also provided valuable
617 input towards their use and fitting. The GGG software suite is maintained
618 by GCT at JPL (tcccon-wiki.caltech.edu). Input on interpreting the results
619 and the spectroscopy in the target region was provided by CDB and GCT.
620 The HITRAN line list is hosted by the Harvard-Smithsonian Center for As-
621 trophysics under the continued direction of Dr Laurence S. Rothman (hitran.org).
622 The GEISA line list is compiled by the Atmospheric Radiation
623 Analysis group at LMD and hosted by the Institut Pierre Simon Laplace ([cds-](http://cds-espri.ipsl.upmc.fr/GEISA/geisa_raie_2015.php)
624 [espri.ipsl.upmc.fr/GEISA/geisa_raie_2015.php](http://cds-espri.ipsl.upmc.fr/GEISA/geisa_raie_2015.php)). Tools hosted by the Earth
625 Observation Data Group were used to reformat the GEISA 2015 line list into
626 the format of the HITRAN line list (eodg.atm.ox.ac.uk/RFM/geihit.html).
627 This work was performed in support of the ExoMars TGO ACS instrument
628 and funded by the National Centre for Space Studies of France (CNES) and
629 the Natural Sciences and Engineering Research Council of Canada (NSERC)
630 (PDF - 516895 - 2018).

631 References

632 Armante, R., Scott, N., Crevoisier, C., Capelle, V., Crepeau, L., Jacquinet,
633 N., Chédin, A., Sep. 2016. Evaluation of spectroscopic databases through
634 radiative transfer simulations compared to observations. Application to the
635 validation of GEISA 2015 with IASI and TCCON. *J. Mol. Spectrosc.* 327,
636 180–192.

- 637 Babikov, Y. L., Mikhailenko, S. N., Barbe, A., Tyuterev, V. G., Sep. 2014.
638 S&MPO - An information system for ozone spectroscopy on the WEB. J.
639 Quant. Spectrosc. Radiat. Transfer 145, 169–196.
- 640 Bailey, J., Jun. 2009. A comparison of water vapor line parameters for mod-
641 eling the Venus deep atmosphere. Icarus 201, 444–453.
- 642 Barbe, A., De Backer, M.-R., Starikova, E., Tashkun, S. A., Thomas, X.,
643 Tyuterev, V. G., Jul. 2012. FTS high resolution spectra of $^{16}\text{O}_3$ in 3500
644 and 5500 cm^{-1} regions. First example of new theoretical modelling for a
645 polyad of strongly coupled states. J. Quant. Spectrosc. Radiat. Transfer
646 113, 829–839.
- 647 Barbe, A., Mikhailenko, S., Starikova, E., De Backer, M.-R., Tyuterev,
648 V. G., Mondelain, D., Kass, S., Campargue, A., Janssen, C., Tashkun, S.,
649 Kochanov, R., Gamache, R., Orphal, J., Nov. 2013. Ozone spectroscopy in
650 the electronic ground state: High-resolution spectra analyses and update
651 of line parameters since 2003. J. Quant. Spectrosc. Radiat. Transfer 130,
652 172–190.
- 653 Barbe, A., Plateaux, J. J., Mikhailenko, S., Tyuterev, V. G., Oct. 1997.
654 Infrared Spectrum of Ozone in the 4600 and 5300 cm^{-1} Regions: High
655 Order Accidental Resonances through the Analysis of $\nu_1 + 2\nu_2 + 3\nu_3 - \nu_2$,
656 $\nu_1 + 2\nu_2 + 3\nu_3$, and $4\nu_1 + \nu_3$ Bands. J. Mol. Spectrosc. 185, 408–416.
- 657 Barber, R. J., Tennyson, J., Harris, G. J., Tolchenov, R. N., May 2006. A
658 high-accuracy computed water line list. Mon. Not. R. Astron. Soc. 368,
659 1087–1094.

660 Bernath, P. F., McElroy, C. T., Abrams, M. C., Boone, C. D., Butler,
 661 M., Camy-Peyret, C., Carleer, M., Clerbaux, C., Coheur, P.-F., Colin,
 662 R., DeCola, P., DeMazière, M., Drummond, J. R., Dufour, D., Evans,
 663 W. F. J., Fast, H., Fussen, D., Gilbert, K., Jennings, D. E., Llewellyn,
 664 E. J., Lowe, R. P., Mahieu, E., McConnell, J. C., McHugh, M., McLeod,
 665 S. D., Michaud, R., Midwinter, C., Nassar, R., Nichitiu, F., Nowlan, C.,
 666 Rinsland, C. P., Rochon, Y. J., Rowlands, N., Semeniuk, K., Simon, P.,
 667 Skelton, R., Sloan, J. J., Soucy, M.-A., Strong, K., Tremblay, P., Turn-
 668 bull, D., Walker, K. A., Walkty, I., Wardle, D. A., Wehrle, V., Zander, R.,
 669 Zou, J., Jun. 2005. Atmospheric Chemistry Experiment (ACE): Mission
 670 overview. *Geophys. Res. Lett.* 32, L15S01.

671 Bertaux, J.-L., Vandaele, A. C., Wilquet, V., Montmessin, F., Dahoo, R.,
 672 Villard, E., Korabiev, O., Fedorova, A., May 2008. First observation of 628
 673 CO₂ isotopologue band at 3.3 μm in the atmosphere of Venus by solar
 674 occultation from Venus Express. *Icarus* 195, 28–33.

675 Birk, M., Wagner, G., Loos, J., Lodi, L., Polyansky, O. L., Kyuberis, A. A.,
 676 Zobov, N. F., Tennyson, J., Dec. 2017. Accurate line intensities for wa-
 677 ter transitions in the infrared: Comparison of theory and experiment. *J.*
 678 *Quant. Spectrosc. Radiat. Transfer* 203, 88–102.

679 Boone, C. D., Nassar, R., Walker, K. A., Rochon, Y., McLeod, S. D., Rins-
 680 land, C. P., Bernath, P. F., Nov. 2005. Retrievals for the atmospheric chem-
 681 istry experiment Fourier-transform spectrometer. *Appl. Opt.* 44, 7218–
 682 7231.

683 Brown, L. R., Sung, K., Benner, D. C., Devi, V. M., Boudon, V., Gabard,
 684 T., Wenger, C., Campargue, A., Leshchishina, O., Kass, S., Monde-
 685 lain, D., Wang, L., Daumont, L., Régalia, L., Rey, M., Thomas, X.,
 686 Tyuterev, V. G., Lyulin, O. M., Nikitin, A. V., Niederer, H. M., Albert,
 687 S., Bauerecker, S., Quack, M., O'Brien, J. J., Gordon, I. E., Rothman,
 688 L. S., Sasada, H., Coustenis, A., Smith, M. A. H., Carrington, T., Wang,
 689 X.-G., Mantz, A. W., Spickler, P. T., Nov. 2013. Methane line parameters
 690 in the HITRAN2012 database. *J. Quant. Spectrosc. Radiat. Transfer* 130,
 691 201–219.

692 Chédin, A., Husson, N., Scott, N. A., Feb. 1982. GEISA - a Data Base for
 693 the Study of Phenomena of Radiative Transfer in Planetary Atmospheres.
 694 *Bulletin d'Information du Centre de Données Stellaires* 22, 121.

695 Clarke, J. T., Mayyasi, M., Bhattacharyya, D., Schneider, N. M., McClint-
 696 tock, W. E., Deighan, J. I., Stewart, A. I. F., Chaufray, J.-Y., Chaffin,
 697 M. S., Jain, S. K., Stiepen, A., Crismani, M., Holsclaw, G. M., Montmessin,
 698 F., Jakosky, B. M., Feb. 2017. Variability of D and H in the Martian upper
 699 atmosphere observed with the MAVEN IUVS echelle channel. *J. Geophys.*
 700 *Res.* 122, 2336–2344.

701 Clerbaux, C., Boynard, A., Clarisse, L., George, M., Hadji-Lazaro, J.,
 702 Herbin, H., Hurtmans, D., Pommier, M., Razavi, A., Turquety, S., We-
 703 spes, C., Coheur, P.-F., Aug. 2009. Monitoring of atmospheric composition
 704 using the thermal infrared IASI/MetOp sounder. *Atmos. Chem. Phys.* 9,
 705 6041–6054.

706 Coudert, L. H., Chelin, P., Aug. 2016. Line position and line intensity anal-
707 yses of the high-resolution spectrum of H_2^{18}O up to the First Triad and J
708 $= 17$. *J. Mol. Spectrosc.* 326, 130–135.

709 Coudert, L. H., Martin-Drumel, M.-A., Pirali, O., Sep. 2014. Analysis of the
710 high-resolution water spectrum up to the Second Triad and to $J = 30$. *J.*
711 *Mol. Spectrosc.* 303, 36–41.

712 Crisp, D., Atlas, R. M., Breon, F.-M., Brown, L. R., Burrows, J. P., Ciais,
713 P., Connor, B. J., Doney, S. C., Fung, I. Y., Jacob, D. J., Miller, C. E.,
714 O’Brien, D., Pawson, S., Randerson, J. T., Rayner, P., Salawitch, R. J.,
715 Sander, S. P., Sen, B., Stephens, G. L., Tans, P. P., Toon, G. C., Wennberg,
716 P. O., Wofsy, S. C., Yung, Y. L., Kuang, Z., Chudasama, B., Sprague, G.,
717 Weiss, B., Pollock, R., Kenyon, D., Schroll, S., Jan. 2004. The Orbiting
718 Carbon Observatory (OCO) mission. *Adv. Space Res.* 34, 700–709.

719 Crisp, D., Pollock, H. R., Rosenberg, R., Chapsky, L., Lee, R. A. M., Oya-
720 fuso, F. A., Frankenberg, C., O’Dell, C. W., Bruegge, C. J., Doran, G. B.,
721 Eldering, A., Fisher, B. M., Fu, D., Gunson, M. R., Mandrake, L., Oster-
722 man, G. B., Schwandner, F. M., Sun, K., Taylor, T. E., Wennberg, P. O.,
723 Wunch, D., Jan. 2017. The on-orbit performance of the Orbiting Car-
724 bon Observatory-2 (OCO-2) instrument and its radiometrically calibrated
725 products. *Atmos. Meas. Tech.* 10, 59–81.

726 Devi, V. M., Benner, D. C., Sung, K., Crawford, T. J., Gamache, R. R.,
727 Renaud, C. L., Smith, M. A. H., Mantz, A. W., Villanueva, G. L., Dec.
728 2017. Line parameters for CO_2 - and self-broadening in the ν_3 band of
729 HD^{16}O . *J. Quant. Spectrosc. Radiat. Transfer* 203, 158–174.

730 Durry, G., Li, J. S., Vinogradov, I., Titov, A., Joly, L., Cousin, J., Decarpen-
 731 terie, T., Amarouche, N., Liu, X., Parvitte, B., Korablev, O., Gerasimov,
 732 M., Zéninari, V., Apr. 2010. Near infrared diode laser spectroscopy of
 733 C₂H₂, H₂O, CO₂ and their isotopologues and the application to TDLAS, a
 734 tunable diode laser spectrometer for the martian PHOBOS-GRUNT space
 735 mission. *Appl. Phys. B* 99, 339–351.

736 Encrenaz, T., DeWitt, C., Richter, M. J., Greathouse, T. K., Fouchet, T.,
 737 Montmessin, F., Lefèvre, F., Bézard, B., Atreya, S. K., Aoki, S., Sagawa,
 738 H., May 2018. New measurements of D/H on Mars using EXES aboard
 739 SOFIA. *Astron. Astrophys.* 612, A112.

740 Formisano, V., Atreya, S., Encrenaz, T., Ignatiev, N., Giuranna, M., Dec.
 741 2004. Detection of Methane in the Atmosphere of Mars. *Science* 306, 1758–
 742 1761.

743 Gamache, R. R., Farese, M., Renaud, C. L., Aug. 2016. A spectral line list
 744 for water isotopologues in the 1100-4100 cm⁻¹ region for application to
 745 CO₂-rich planetary atmospheres. *J. Mol. Spectrosc.* 326, 144–150.

746 Giuranna, M., Viscardy, S., Daerden, F., Neary, L., Etiope, G., Oehler,
 747 D., Formisano, V., Aronica, A., Wolkenberg, P. and Aoki, S., Cardes-
 748 Moinelo, A., Marn-Yaseli de la Parra, J., Merritt, D., Amoroso, M., 2019.
 749 Independent confirmation of a methane spike on Mars and a source region
 750 east of Gale Crater. *Nat. Geosci.*, 1752–0908.

751 Gordon, I. E., Rothman, L. S., Hill, C., Kochanov, R. V., Tan, Y., Bernath,
 752 P. F., Birk, M., Boudon, V., Campargue, A., Chance, K. V., Drouin, B. J.,

753 Flaud, J.-M., Gamache, R. R., Hodges, J. T., Jacquemart, D., Perevalov,
 754 V. I., Perrin, A., Shine, K. P., Smith, M.-A. H., Tennyson, J., Toon,
 755 G. C., Tran, H., Tyuterev, V. G., Barbe, A., Császár, A. G., Devi, V. M.,
 756 Furtenbacher, T., Harrison, J. J., Hartmann, J.-M., Jolly, A., Johnson,
 757 T. J., Karman, T., Kleiner, I., Kyuberis, A. A., Loos, J., Lyulin, O. M.,
 758 Massie, S. T., Mikhailenko, S. N., Moazzen-Ahmadi, N., Müller, H. S. P.,
 759 Naumenko, O. V., Nikitin, A. V., Polyansky, O. L., Rey, M., Rotger, M.,
 760 Sharpe, S. W., Sung, K., Starikova, E., Tashkun, S. A., Auwera, J. V.,
 761 Wagner, G., Wilzewski, J., Wcisło, P., Yu, S., Zak, E. J., Dec. 2017.
 762 The HITRAN2016 molecular spectroscopic database. *J. Quant. Spectrosc.*
 763 *Radiat. Transfer* 203, 3–69.

764 Huang, X., Gamache, R. R., Freedman, R. S., Schwenke, D. W., Lee, T. J.,
 765 Nov. 2014. Reliable infrared line lists for 13 CO₂ isotopologues up to
 766 $E'=18,000\text{ cm}^{-1}$ and 1500 K, with line shape parameters. *J. Quant. Spec-*
 767 *trosc. Radiat. Transfer* 147, 134–144.

768 Irion, F. W., Gunson, M. R., Toon, G. C., Chang, A. Y., Eldering, A.,
 769 Mahieu, E., Manney, G. L., Michelsen, H. A., Moyer, E. J., Newchurch,
 770 M. J., Osterman, G. B., Rinsland, C. P., Salawitch, R. J., Sen, B., Yung,
 771 Y. L., Zander, R., Nov. 2002. Atmospheric Trace Molecule Spectroscopy
 772 (ATMOS) Experiment Version 3 data retrievals. *Appl. Opt.* 41, 6968–6979.

773 Jacquemart, D., Gueye, F., Lyulin, O. M., Karlovets, E. V., Baron, D.,
 774 Perevalov, V. I., Jul. 2012. Infrared spectroscopy of CO₂ isotopologues
 775 from 2200 to 7000 cm^{-1} : I-Characterizing experimental uncertainties of

776 positions and intensities. *J. Quant. Spectrosc. Radiat. Transfer* 113, 961–
777 975.

778 Jacquinet-Husson, N., Armante, R., Scott, N. A., Chédin, A., Crépeau, L.,
779 Boutammine, C., Bouhdaoui, A., Crevoisier, C., Capelle, V., Boone, C.,
780 Poulet-Crovisier, N., Barbe, A., Chris Benner, D., Boudon, V., Brown,
781 L. R., Buldyreva, J., Campargue, A., Coudert, L. H., Devi, V. M., Down,
782 M. J., Drouin, B. J., Fayt, A., Fittschen, C., Flaud, J.-M., Gamache,
783 R. R., Harrison, J. J., Hill, C., Hodnebrog, Ø., Hu, S.-M., Jacquemart, D.,
784 Jolly, A., Jiménez, E., Lavrentieva, N. N., Liu, A.-W., Lodi, L., Lyulin,
785 O. M., Massie, S. T., Mikhailenko, S., Müller, H. S. P., Naumenko, O. V.,
786 Nikitin, A., Nielsen, C. J., Orphal, J., Perevalov, V. I., Perrin, A., Polovt-
787 seva, E., Predoi-Cross, A., Rotger, M., Ruth, A. A., Yu, S. S., Sung,
788 K., Tashkun, S. A., Tennyson, J., Tyuterev, V. G., Vander Auwera, J.,
789 Voronin, B. A., Makie, A., Sep. 2016. The 2015 edition of the GEISA
790 spectroscopic database. *J. Mol. Spectrosc.* 327, 31–72.

791 Johnson, T. J., Profeta, L. T. M., Sams, R. L., Griffith, D. W. T., Yokel-
792 son, R. L., May 2010. An infrared spectral database for detection of gases
793 emitted by biomass burning. *Vib. Spectrosc.* 53, 97–102.

794 Kalnay, E., Kanamitsu, M., Kistler, R., Collins, W., Deaven, D., Gandin,
795 L., Iredell, M., Saha, S., White, G., Woollen, J., Zhu, Y., Leetmaa, A.,
796 Reynolds, B., Chelliah, M., Ebisuzaki, W., Higgins, W., Janowiak, J.,
797 Mo, K. C., Ropelewski, C., Wang, J., Jenne, R., Joseph, D., Mar. 1996.
798 The NCEP/NCAR 40-Year Reanalysis Project. *Bull. Am. Astron. Soc.* 77,
799 437–472.

800 Korablev, O., Montmessin, F., Trokhimovskiy, A., Fedorova, A. A., Shakun,
 801 A. V., Grigoriev, A. V., Moshkin, B. E., Ignatiev, N. I., Forget, F., Lefèvre,
 802 F., Anufreychik, K., Dzuban, I., Ivanov, Y. S., Kalinnikov, Y. K., Ko-
 803 zlova, T. O., Kungurov, A., Makarov, V., Martynovich, F., Maslov, I.,
 804 Merzlyakov, D., Moiseev, P. P., Nikolskiy, Y., Patrakeev, A., Patsaev, D.,
 805 Santos-Skripko, A., Sazonov, O., Semena, N., Semenov, A., Shashkin, V.,
 806 Sidorov, A., Stepanov, A. V., Stupin, I., Timonin, D., Titov, A. Y., Vik-
 807 torov, A., Zharkov, A., Altieri, F., Arnold, G., Belyaev, D. A., Bertaux,
 808 J. L., Betsis, D. S., Duxbury, N., Encrenaz, T., Fouchet, T., Gérard,
 809 J.-C., Grassi, D., Guerlet, S., Hartogh, P., Kasaba, Y., Khatuntsev, I.,
 810 Krasnopolsky, V. A., Kuzmin, R. O., Lellouch, E., Lopez-Valverde, M. A.,
 811 Luginin, M., Määttänen, A., Marcq, E., Martin Torres, J., Medvedev,
 812 A. S., Millour, E., Olsen, K. S., Patel, M. R., Quantin-Nataf, C., Rodin,
 813 A. V., Shematovich, V. I., Thomas, I., Thomas, N., Vazquez, L., Vin-
 814 cendon, M., Wilquet, V., Wilson, C. F., Zasova, L. V., Zelenyi, L. M.,
 815 Zorzano, M. P., Feb. 2018. The Atmospheric Chemistry Suite (ACS) of
 816 Three Spectrometers for the ExoMars 2016 Trace Gas Orbiter. *Space Sci.*
 817 *Rev.* 214, 7.

818 Korablev, O., Vandaele, A. C., Montmessin, F., Fedorova, A. A., Trokhi-
 819 movskiy, A., Forget, F., Lefèvre, F., Daerden, F., Thomas, I. R., Trompet,
 820 L., Erwin, J. T., Aoki, S., Robert, S., Neary, L., Viscardy, S., Grigoriev,
 821 A., Ignatiev, N., Shakun, A., Patrakeev, A., Belyaev, D., Bertaux, J.-L.,
 822 Olsen, K. S., Baggio, L., Alday, J., Ivanov, Y. S., Bojan, R., et al., 2019.
 823 No detection of methane on Mars from early ExoMars Trace Gas Orbiter
 824 observations. *Nature*.

- 825 Krasnopolsky, V. A., Sep. 2015. Variations of the HDO/H₂O ratio in the
826 martian atmosphere and loss of water from Mars. *Icarus* 257, 377–386.
- 827 Krasnopolsky, V. A., Maillard, J. P., Owen, T. C., Dec. 2004. Detection of
828 methane in the Martian atmosphere: evidence for life? *Icarus* 172, 537–
829 547.
- 830 Li, G., Gordon, I. E., Hajigeorgiou, P. G., Coxon, J. A., Rothman, L. S.,
831 Nov 2013. Reference spectroscopic data for hydrogen halides, Part II: The
832 line lists. *J. Quant. Spectrosc. Radiat. Transfer* 130, 284–295.
- 833 Li, G., Gordon, I. E., Rothman, L. S., Tan, Y., Hu, S.-M., Kassi, S., Cam-
834 pargue, A., Medvedev, E. S., Jan. 2015. Rovibrational Line Lists for Nine
835 Isotopologues of the CO Molecule in the X ¹Σ⁺ Ground Electronic State.
836 *Astrophys. J. Suppl. Ser.* 216, 15.
- 837 Lodi, L., Tennyson, J., Jul. 2012. Line lists for H₂¹⁸O and H₂¹⁷O based
838 on empirical line positions and ab initio intensities. *J. Quant. Spectrosc.*
839 *Radiat. Transfer* 113, 850–858.
- 840 Lodi, L., Tennyson, J., Polyansky, O. L., Jul. 2011. A global, high accuracy
841 ab initio dipole moment surface for the electronic ground state of the water
842 molecule. *J. Chem. Phys.* 135 (3), 034113–034113.
- 843 Loos, J., Birk, M., Wagner, G., Dec. 2017a. Measurement of air-broadening
844 line shape parameters and temperature dependence parameters of H₂O
845 lines in the spectral ranges 1850-2280 cm⁻¹ and 2390-4000 cm⁻¹. *J. Quant.*
846 *Spectrosc. Radiat. Transfer* 203, 103–118.

- 847 Loos, J., Birk, M., Wagner, G., Dec. 2017b. Measurement of positions, in-
848 tensities and self-broadening line shape parameters of H₂O lines in the
849 spectral ranges 1850-2280 cm⁻¹ and 2390-4000 cm⁻¹. J. Quant. Spectrosc.
850 Radiat. Transfer 203, 119–132.
- 851 Lyulin, O. M., Karlovets, E. V., Jacquemart, D., Lu, Y., Liu, A. W.,
852 Perevalov, V. I., Nov. 2012. Infrared spectroscopy of 17O- and 18O-
853 enriched carbon dioxide in the 1700-8300cm⁻¹ wavenumber region. J.
854 Quant. Spectrosc. Radiat. Transfer 113, 2167–2181.
- 855 McClatchey, R. A., Benedict, W. S., Clough, S. A., Burch, D. E., Calfee,
856 R. F., Fox, K., Rothman, L. S., Garing, J. S., 1973. AFCRL atmospheric
857 absorption line parameters compilation. Air Force Cambridge Research
858 Laboratories, Bedford, Ma.
- 859 Mendonca, J., Strong, K., Toon, G. C., Wunch, D., Sung, K., Deutscher,
860 N. M., Griffith, D. W. T., Franklin, J. E., May 2016. Improving atmo-
861 spheric CO₂ retrievals using line mixing and speed-dependence when fit-
862 ting high-resolution ground-based solar spectra. J. Mol. Spectrosc. 323,
863 15–27.
- 864 Mumma, M. J., Villanueva, G. L., Novak, R. E., Hewagama, T., Bonev, B. P.,
865 DiSanti, M. A., Mandell, A. M., Smith, M. D., Feb. 2009. Strong Release
866 of Methane on Mars in Northern Summer 2003. Science 323, 1041–1045.
- 867 Niederer, H.-M., Wang, X.-G., Carrington, T., Albert, S., Bauerecker, S.,
868 Boudon, V., Quack, M., Sep. 2013. Analysis of the rovibrational spectrum
869 of ¹³CH₄ in the Octad range. J. Mol. Spectrosc. 291, 33–47.

870 Nikitin, A. V., Boudon, V., Wenger, C., Albert, S., Brown, L. R., Bauerecker,
871 S., Quack, M., 2013. High resolution spectroscopy and the first global
872 analysis of the Tetradecad region of methane $^{12}\text{CH}_4$. *Phys. Chem. Chem.*
873 *Phys.* 15, 10071.

874 Norton, R. H., Rinsland, C. P., Feb. 1991. ATMOS data processing and
875 science analysis methods. *Appl. Opt.* 30, 389–400.

876 Olsen, K. S., Toon, G. C., Boone, C. D., Strong, K., 2015. New temper-
877 ature and pressure retrieval algorithm for high-resolution infrared solar
878 occultation spectrometry: analysis and validation against ACE-FTS and
879 COSMIC. *Atmos. Meas. Tech. Disc.* 8, 10823–10873.

880 Rothman, L. S., Gamache, R. R., Tipping, R. H., Rinsland, C. P., Smith,
881 M. A. H., Benner, D. C., Devi, V. M., Flaud, J.-M., Camy-Peyret, C.,
882 Perrin, A., 1992. The HITRAN molecular data base - Editions of 1991 and
883 1992. *J. Quant. Spectrosc. Radiat. Transfer* 48, 469–507.

884 Rothman, L. S., Gordon, I. E., Babikov, Y., Barbe, A., Chris Benner, D.,
885 Bernath, P. F., Birk, M., Bizzocchi, L., Boudon, V., Brown, L. R., Cam-
886 pargue, A., Chance, K., Cohen, E. A., Coudert, L. H., Devi, V. M., Drouin,
887 B. J., Fayt, A., Flaud, J.-M., Gamache, R. R., Harrison, J. J., Hartmann,
888 J.-M., Hill, C., Hodges, J. T., Jacquemart, D., Jolly, A., Lamouroux, J., Le
889 Roy, R. J., Li, G., Long, D. A., Lyulin, O. M., Mackie, C. J., Massie, S. T.,
890 Mikhailenko, S., Müller, H. S. P., Naumenko, O. V., Nikitin, A. V., Or-
891 phal, J., Perevalov, V., Perrin, A., Polovtseva, E. R., Richard, C., Smith,
892 M. A. H., Starikova, E., Sung, K., Tashkun, S., Tennyson, J., Toon, G. C.,

893 Tyuterev, V. G., Wagner, G., Nov. 2013. The HITRAN2012 molecular
894 spectroscopic database. *J. Quant. Spectrosc. Radiat. Transfer* 130, 4–50.

895 Rothman, L. S., Gordon, I. E., Barbe, A., Benner, D. C., Bernath, P. F.,
896 Birk, M., Boudon, V., Brown, L. R., Campargue, A., Champion, J.-P.,
897 Chance, K., Coudert, L. H., Dana, V., Devi, V. M., Fally, S., Flaud, J.-
898 M., Gamache, R. R., Goldman, A., Jacquemart, D., Kleiner, I., Lacome,
899 N., Lafferty, W. J., Mandin, J.-Y., Massie, S. T., Mikhailenko, S. N.,
900 Miller, C. E., Moazzen-Ahmadi, N., Naumenko, O. V., Nikitin, A. V.,
901 Orphal, J., Perevalov, V. I., Perrin, A., Predoi-Cross, A., Rinsland, C. P.,
902 Rotger, M., Šimečková, M., Smith, M. A. H., Sung, K., Tashkun, S. A.,
903 Tennyson, J., Toth, R. A., Vandaele, A. C., Vander Auwera, J., Jun. 2009.
904 The HITRAN 2008 molecular spectroscopic database. *J. Quant. Spectrosc.*
905 *Radiat. Transfer* 110, 533–572.

906 Sen, B., Toon, G. C., Blavier, J.-F., Fleming, E. L., Jackman, C. H., Apr.
907 1996. Balloon-borne observations of midlatitude fluorine abundance. *J.*
908 *Geophys. Res.* 101, 9045–9054.

909 Sharpe, S. W., Johnson, T. J., Sams, R. L., Chu, P. M., Rhoderick, G. C.,
910 Johnson, P. A., Dec. 2004. Gas-Phase Databases for Quantitative Infrared
911 Spectroscopy. *Appl. Spectrosc.* 58, 1452–1461.

912 Tashkun, S. A., Perevalov, V. I., Gamache, R. R., Lamouroux, J., Feb. 2015.
913 CDSD-296, high resolution carbon dioxide spectroscopic databank: Ver-
914 sion for atmospheric applications. *J. Quant. Spectrosc. Radiat. Transfer*
915 152, 45–73.

916 Tennyson, J., Bernath, P. F., Brown, L. R., Campargue, A., Carleer, M. R.,
 917 Császár, A. G., Gamache, R. R., Hodges, J. T., Jenouvrier, A., Naumenko,
 918 O. V., Polyansky, O. L., Rothman, L. S., Toth, R. A., Carine Vandaele, A.,
 919 Zobov, N. F., Daumont, L., Fazliev, A. Z., Furtenbacher, T., Gordon, I. E.,
 920 Mikhailenko, S. N., Shirin, S. V., Jun. 2009. IUPAC critical evaluation of
 921 the rotational-vibrational spectra of water vapor. Part I—Energy levels and
 922 transition wavenumbers for H₂¹⁷O and H₂¹⁸O. J. Quant. Spectrosc. Radiat.
 923 Transfer 110, 573–596.

924 Toon, G., 2019. CO₂ Spectroscopy Evaluation: 670 to 7000 cm⁻¹. Tech.
 925 rep., Jet Propulsion Laboratory.
 926 URL [mark4sun.jpl.nasa.gov/toon/atm18/NDACC_TCCON_2019_](http://mark4sun.jpl.nasa.gov/toon/atm18/NDACC_TCCON_2019_Toon-compressed.pdf)
 927 [Toon-compressed.pdf](http://mark4sun.jpl.nasa.gov/toon/atm18/NDACC_TCCON_2019_Toon-compressed.pdf)

928 Toon, G. C., Oct. 1991. The JPL MkIV interferometer. Opt. Photonics News
 929 2, 19–21.

930 Toon, G. C., Blavier, J.-F., Sung, K., Rothman, L. S., E. Gordon, I., Oct.
 931 2016. HITRAN spectroscopy evaluation using solar occultation FTIR spec-
 932 tra. J. Quant. Spectrosc. Radiat. Transfer 182, 324–336.

933 Toth, R. A., Brown, L. R., Miller, C. E., Malathy Devi, V., Benner, D. C.,
 934 Apr. 2008a. Spectroscopic database of CO₂ line parameters: 4300 7000
 935 cm⁻¹. J. Quant. Spectrosc. Radiat. Transfer 109, 906–921.

936 Toth, R. A., Miller, C. E., Brown, L. R., Devi, V. M., Benner, D. C., May
 937 2007. Line positions and strengths of ¹⁶O ¹²C ¹⁸O, ¹⁸O ¹²C ¹⁸O and ¹⁷O
 938 ¹²C ¹⁸O between 2200 and 7000 cm⁻¹. J. Mol. Spectrosc. 243, 43–61.

939 Toth, R. A., Miller, C. E., Brown, L. R., Devi, V. M., Benner, D. C., Sep.
 940 2008b. Line strengths of $^{16}\text{O }^{13}\text{C }^{16}\text{O}$, $^{16}\text{O }^{13}\text{C }^{18}\text{O}$, $^{16}\text{O }^{13}\text{C }^{17}\text{O}$ and ^{18}O
 941 $^{13}\text{C }^{18}\text{O}$ between 2200 and 6800 cm^{-1} . *J. Mol. Spectrosc.* 251, 64–89.

942 Tyuterev, V., Tashkun, S., Rey, M., Kochanov, R., Nikitin, A., Delahaye, T.,
 943 Dec. 2013. Accurate Spectroscopic Models for Methane Polyads Derived
 944 from a Potential Energy Surface Using High-Order Contact Transforma-
 945 tions. *J. Phys. Chem. A* 117, 13779–13805.

946 Vandaele, A. C., Lopez-Moreno, J.-J., Patel, M. R., Bellucci, G., Daer-
 947 den, F., Ristic, B., Robert, S., Thomas, I. R., Wilquet, V., Allen, M.,
 948 Alonso-Rodrigo, G., Altieri, F., Aoki, S., Bolsée, D., Clancy, T., Cloutis,
 949 E., Depiesse, C., Drummond, R., Fedorova, A., Formisano, V., Funke,
 950 B., González-Galindo, F., Geminale, A., Gérard, J.-C., Giuranna, M.,
 951 Hetey, L., Ignatiev, N., Kaminski, J., Karatekin, O., Kasaba, Y., Leese,
 952 M., Lefèvre, F., Lewis, S. R., López-Puertas, M., López-Valverde, M.,
 953 Mahieux, A., Mason, J., McConnell, J., Mumma, M., Neary, L., Neefs,
 954 E., Renotte, E., Rodriguez-Gomez, J., Sindoni, G., Smith, M., Stiepen,
 955 A., Trokhimovsky, A., Vander Auwera, J., Villanueva, G., Viscardy, S.,
 956 Whiteway, J., Willame, Y., Wolff, M., Aug. 2018. NOMAD, an Integrated
 957 Suite of Three Spectrometers for the ExoMars Trace Gas Mission: Techni-
 958 cal Description, Science Objectives and Expected Performance. *Space Sci.*
 959 *Rev.* 214, 80.

960 Vandaele, A. C., Neefs, E., Drummond, R., Thomas, I. R., Daerden, F.,
 961 Lopez-Moreno, J.-J., Rodriguez, J., Patel, M. R., Bellucci, G., Allen, M.,
 962 Altieri, F., Bolsée, D., Clancy, T., Delanoye, S., Depiesse, C., Cloutis, E.,

963 Fedorova, A., Formisano, V., Funke, B., Fussen, D., Geminale, A., Gérard,
 964 J.-C., Giuranna, M., Ignatiev, N., Kaminski, J., Karatekin, O., Lefèvre,
 965 F., López-Puertas, M., López-Valverde, M., Mahieux, A., McConnell, J.,
 966 Mumma, M., Neary, L., Renotte, E., Ristic, B., Robert, S., Smith, M.,
 967 Trokhimovsky, S., Vander Auwera, J., Villanueva, G., Whiteway, J., Wil-
 968 quet, V., Wolff, M., Dec. 2015. Science objectives and performances of
 969 NOMAD, a spectrometer suite for the ExoMars TGO mission. *Planet.*
 970 *Space Sci.* 119, 233–249.

971 Villanueva, G. L., Mumma, M. J., Novak, R. E., Hewagama, T., May 2008.
 972 Identification of a new band system of isotopic CO₂ near 3.3 μ m: Impli-
 973 cations for remote sensing of biomarker gases on Mars. *Icarus* 195, 34–44.

974 Webster, C. R., Mahaffy, P. R., Atreya, S. K., Flesch, G. J., Mischna, M. A.,
 975 Meslin, P.-Y., Farley, K. A., Conrad, P. G., Christensen, L. E., Pavlov,
 976 A. A., et al., Jan. 2015. Mars methane detection and variability at Gale
 977 crater. *Science* 347, 415–417.

978 Webster, C. R., Mahaffy, P. R., Atreya, S. K., Moores, J. E., Flesch, G. J.,
 979 Malespin, C., McKay, C. P., Martinez, G., Smith, C. L., Martin-Torres,
 980 J., Gomez-Elvira, J., Zorzano, M.-P., Wong, M. H., Trainer, M. G., Steele,
 981 A., Archer, D., Sutter, B., Coll, P. J., Freissinet, C., Meslin, P.-Y., Gough,
 982 R. V., House, C. H., Pavlov, A., Eigenbrode, J. L., Glavin, D. P., Pear-
 983 son, J. C., Keymeulen, D., Christensen, L. E., Schwenzer, S. P., Navarro-
 984 Gonzalez, R., Pla-García, J., Rafkin, S. C. R., Vicente-Retortillo, Á., Ka-
 985 hanpää, H., Viudez-Moreiras, D., Smith, M. D., Harri, A.-M., Genzer,
 986 M., Hassler, D. M., Lemmon, M., Crisp, J., Sander, S. P., Zurek, R. W.,

- 987 Vasavada, A. R., Jun. 2018. Background levels of methane in Mars' atmo-
988 sphere show strong seasonal variations. *Science* 360, 1093–1096.
- 989 Wilzewski, J. S., Gordon, I. E., Kochanov, R. V., Hill, C., Rothman, L. S.,
990 Jan. 2016. H₂, He, and CO₂ line-broadening coefficients, pressure shifts
991 and temperature-dependence exponents for the HITRAN database. Part
992 1: SO₂, NH₃, HF, HCl, OCS and C₂H₂. *J. Quant. Spectrosc. Radiat.*
993 *Transfer* 168, 193–206.
- 994 Wunch, D., Toon, G. C., Blavier, J. L., Washenfelder, R. A., Notholt, J.,
995 Connor, B. J., Griffith, D. W. T., Sherlock, V., Wennberg, P. O., May
996 2011. The Total Carbon Column Observing Network. *Phil. Trans. R. Soc.*
997 *A* 369, 2087–2112.
- 998 Yokota, T., Yoshida, Y., Eguchi, N., Ota, Y., Tanaka, T., Watanabe, H.,
999 Maksyutov, S., 2009. Global concentrations of CO₂ and CH₄ retrieved from
1000 gosat: First preliminary results. *Sci. Online Lett. Atmos.* 5, 160–163.
- 1001 Zak, E., Tennyson, J., Polyansky, O. L., Lodi, L., Zobov, N. F., Tashkun,
1002 S. A., Perevalov, V. I., Jul. 2016. A room temperature CO₂ line list with
1003 ab initio computed intensities. *J. Quant. Spectrosc. Radiat. Transfer* 177,
1004 31–42.
- 1005 Zurek, R. W., Chicarro, A., Allen, M. A., Bertaux, J.-L., Clancy, R. T.,
1006 Daerden, F., Formisano, V., Garvin, J. B., Neukum, G., Smith, M. D.,
1007 Feb. 2011. Assessment of a 2016 mission concept: The search for trace
1008 gases in the atmosphere of Mars. *Planet. Space Sci.* 59, 284–291.

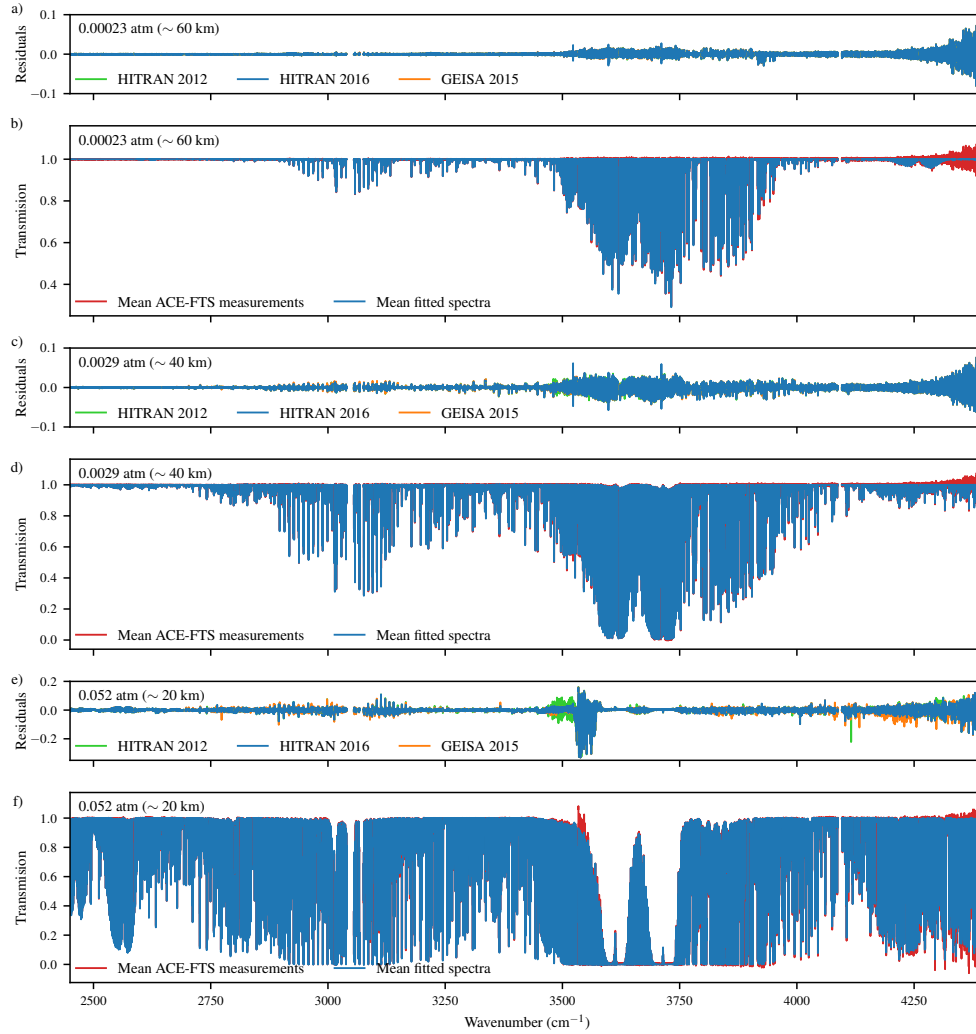


Figure 2: Mean ACE-FTS spectra, mean best-fit computed spectra, and mean residuals for each fitting window. Mean residuals are shown using HITRAN 2012 (green), HITRAN 2016 (blue) and GEISA 2015 (orange). Mean fitted spectra are shown only for when using HITRAN 2016. a) mean residuals from 0.00023 atm (~ 60 km), b) mean spectra and mean fits from 0.00023 atm, c) mean residuals from 0.0029 atm (~ 40 km), d) mean spectra and mean fits from 0.0029 atm, e) mean residuals from 0.052 atm (~ 20 km), f) mean spectra and mean fits from 0.052 atm.

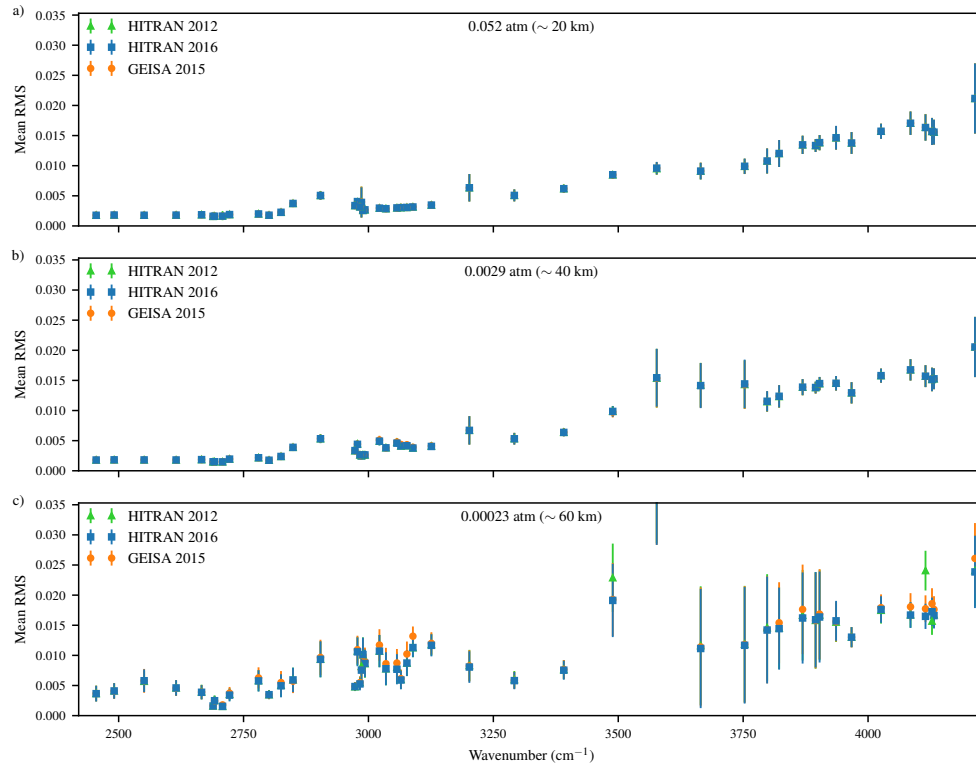


Figure 3: Mean RMS values computes for each fitting window when using each HITRAN 2012, HITRAN 2016, and GEISA 2015 at three pressure levels: a) 0.00023 atm (~ 60 km), b) 0.0029 atm (~ 40 km), c) 0.052 atm (~ 20 km).

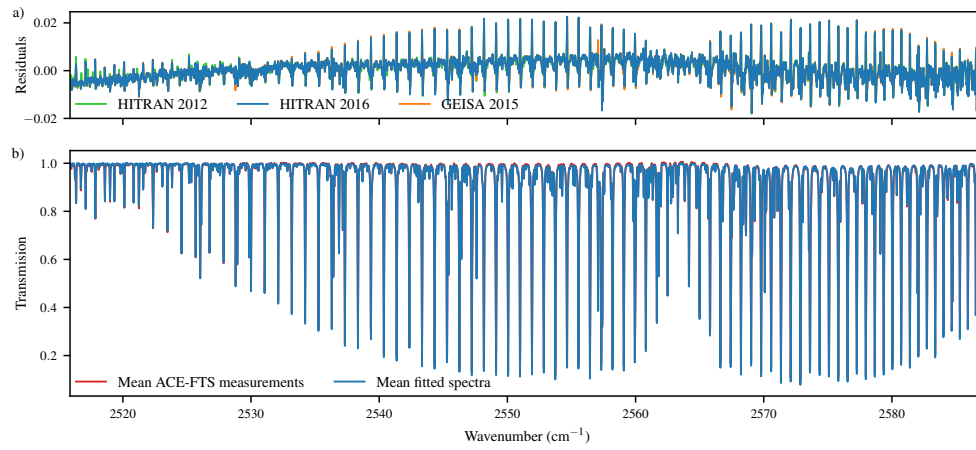


Figure 4: a) Mean residuals for the 2551.55 cm^{-1} window at 0.052 atm ($\sim 20 \text{ km}$) with HITRAN 2012, HITRAN 2016, and GEISA 2015. b) Mean measured ACE-FTS spectrum and mean computed spectrum (for HITRAN 2016). The primary features in this window are N_2O lines and the residuals correspond to the N_2O lines.

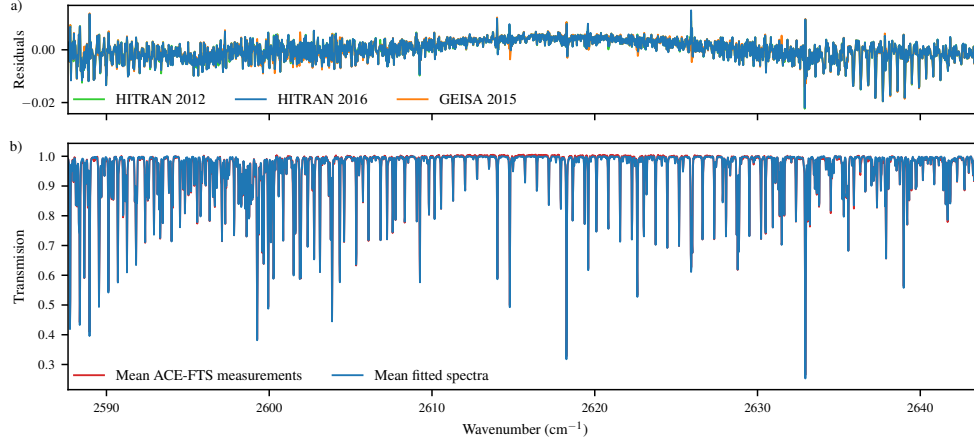


Figure 5: a) Mean residuals for the 2615.74 cm⁻¹ window at 0.052 atm (~20 km) with HITRAN 2012, HITRAN 2016, and GEISA 2015. b) Mean measured ACE-FTS spectrum and mean computed spectrum (for HITRAN 2016). The main features are from N₂O towards the left edge, a CO₂ band across the entire window, and several strong CH₄ lines. The residuals are due to HNO₃.

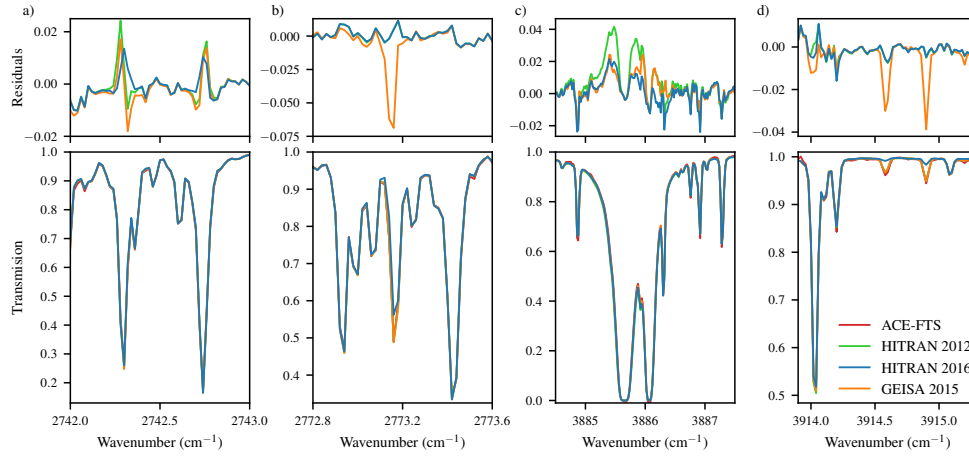


Figure 6: Zoom of the residuals and mean spectra (as in Figures 4 and 5) where errors are present, for the windows: a) 2722.25 cm⁻¹, b) 2780.74 cm⁻¹, c) 3869.14 cm⁻¹, d) 3936.15 cm⁻¹.

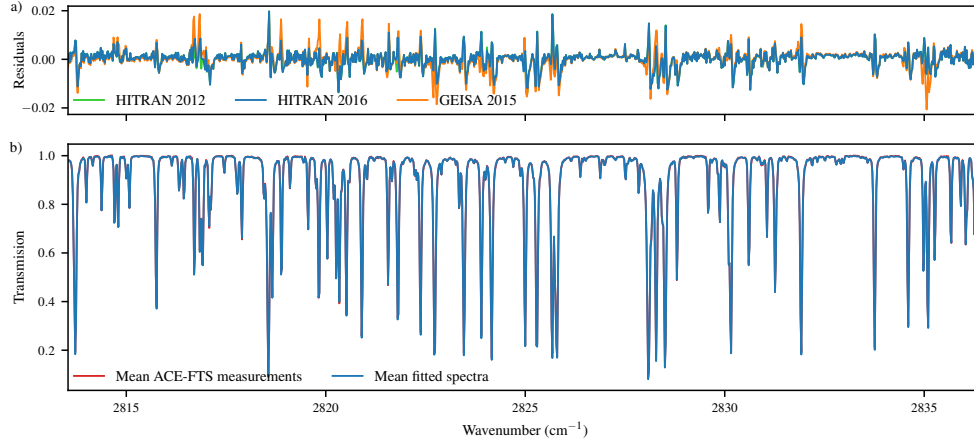


Figure 7: a) Mean residuals for the 2825.0 cm⁻¹ window at 0.052 atm (~20 km) with HITRAN 2012, HITRAN 2016, and GEISA 2015. b) Mean measured ACE-FTS spectrum and mean computed spectrum (for HITRAN 2016). Features are primarily CH₄ lines.

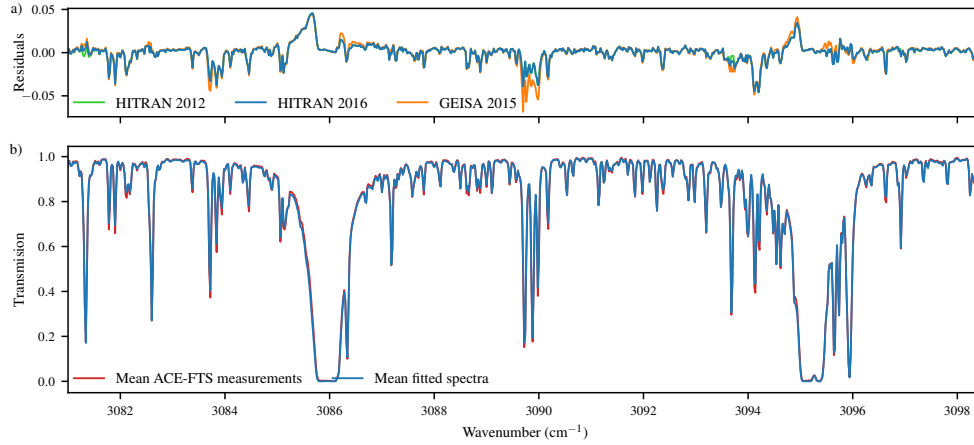


Figure 8: a) Mean residuals for the 3089.75 cm⁻¹ window at 0.052 atm (~20 km) with HITRAN 2012, HITRAN 2016, and GEISA 2015. b) Mean measured ACE-FTS spectrum and mean computed spectrum (for HITRAN 2016). Absorption are due to, in order of prominence, CH₄, H₂O, and O₃. Large residuals near 3090 cm⁻¹ are from CH₄ lines.

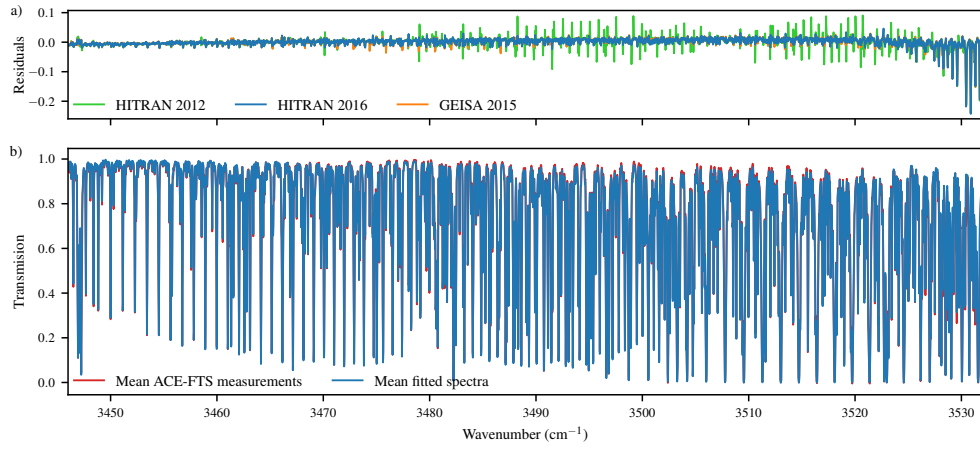


Figure 9: a) Mean residuals for the 3489.0 cm^{-1} window at 0.052 atm ($\sim 20 \text{ km}$) with HITRAN 2012, HITRAN 2016, and GEISA 2015. b) Mean measured ACE-FTS spectrum and mean computed spectrum (for HITRAN 2016). The primary features are an N_2O band on the left side, CO_2 bands on the right, and several H_2O lines. The strong residuals are due to CO_2 when using the HITRAN 2012 line list.

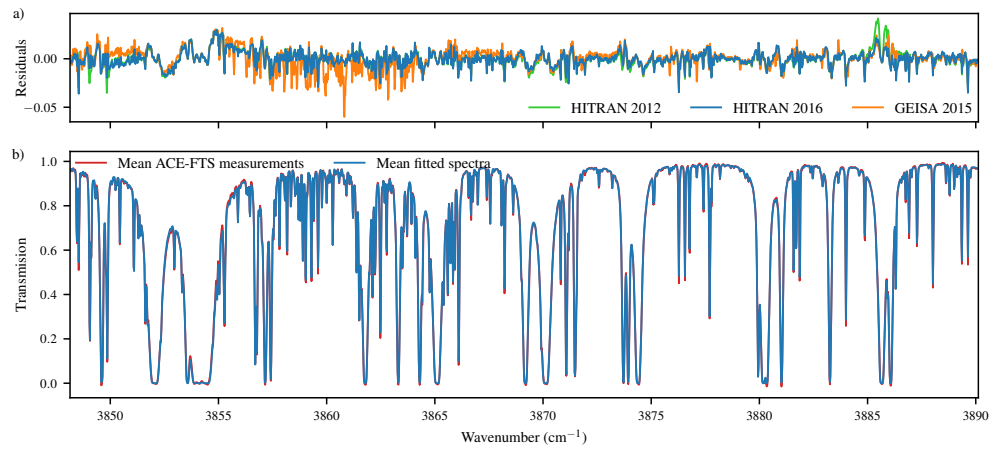


Figure 10: a) Mean residuals for the 3869.14 cm^{-1} window at 0.052 atm ($\sim 20 \text{ km}$) with HITRAN 2012, HITRAN 2016, and GEISA 2015. b) Mean measured ACE-FTS spectrum and mean computed spectrum (for HITRAN 2016). The primary features are H_2O lines. The strong residuals near 3860 cm^{-1} are due to O_3 when using GEISA 2015. Those near 3886 cm^{-1} are due to H_2O and are shown in Figure 6c.